



HAL
open science

Lateral-torsional buckling of uniform and tapered welded I-section beams

Maxime Lebastard, Maël Couchaux, Alain Bureau, Mohammed Hjiiaj

► **To cite this version:**

Maxime Lebastard, Maël Couchaux, Alain Bureau, Mohammed Hjiiaj. Lateral-torsional buckling of uniform and tapered welded I-section beams. *Engineering Structures*, 2024, 303, pp.117301. 10.1016/j.engstruct.2023.117301 . hal-04485661

HAL Id: hal-04485661

<https://univ-rennes.hal.science/hal-04485661v1>

Submitted on 25 Apr 2024

HAL is a multi-disciplinary open access archive for the deposit and dissemination of scientific research documents, whether they are published or not. The documents may come from teaching and research institutions in France or abroad, or from public or private research centers.

L'archive ouverte pluridisciplinaire **HAL**, est destinée au dépôt et à la diffusion de documents scientifiques de niveau recherche, publiés ou non, émanant des établissements d'enseignement et de recherche français ou étrangers, des laboratoires publics ou privés.



Distributed under a Creative Commons Attribution - NonCommercial 4.0 International License

Lateral-torsional buckling of uniform and tapered welded I-section beams

Maxime Lebastard^{a,b}, Maël Couchaux^b, Alain Bureau^a, Mohammed Hjjaj^b.

^a: Centre Technique Industriel de la Construction Métallique, Espace technologique – L’Orme des Merisiers – Immeuble Apollo, 91190 Saint-Aubin, France

^b: Institut National des Sciences Appliquées – 20 Avenue des Buttes de Coësmes, 35708 Rennes, France

ABSTRACT

The current Eurocode 3 rules for buckling of welded I-section members are based on the assumption of hot-rolled flanges. However, flame-cut flanges are widely used in practise and induce significantly different residual stress distributions, affecting the lateral-torsional buckling resistance. Experimental tests and finite element analyses considering residual stress distributions clearly highlighted the beneficial effect of flame-cut flanges compared with hot-rolled flanges on the lateral-torsional buckling resistance of welded I-beams. To complete these preliminary results, a large number of non-linear finite element analyses are performed considering welded beams made of hot-rolled or flame-cut flanges. The beams are composed of steel grades S275 and S355. Numerical results confirm the influence of the flange fabrication process on the buckling behaviour. Eurocode 3 rules are found to be overly conservative for welded beams made of flame-cut flanges. Consequently, proposals are made that are more suitable for estimates of the lateral-torsional buckling resistance of welded beams made of flame-cut flanges. The code rules are also very conservative for welded beams made of hot-rolled flanges with a medium-to-high slenderness. A design method is thus proposed to improve the prediction accuracy of the lateral-torsional buckling resistance of slender welded beams made of hot-rolled flanges.

The novel design method from prEurocode 3 provides acceptable values of the buckling resistance for welded beams made of flame-cut flanges but is restricted to uniform doubly symmetric beams.

An extension of its scope to mono-symmetric uniform beams as well as tapered beams is thus

28 suggested. An enhanced imperfection factor is proposed, adapted to welded beams made of flame-
29 cut flanges.

30 *Keywords: Lateral-torsional buckling, Flame-cut flanges, Tapered beams, Mono-symmetric*
31 *beams.*

32 **1 INTRODUCTION**

33 The lateral-torsional buckling resistance of a steel beam is influenced by the cross-sectional
34 bending resistance, the slenderness and the imperfections resulting from the fabrication process.

35 For welded members, the future and current Eurocode 3 Part 1-1 ([1], [2]) rules were developed
36 considering hot-rolled flanges for which the fabrication process does not includes thermal cuts,
37 hereafter referred to as “*hot-rolled flanges*”. However, other fabrication methods are widely used
38 in practise, especially flame-cut flanges. Both fabrication methods induce significantly different
39 residual stress distributions ([3], [4]). These differences yield substantial deviations in the lateral-
40 torsional buckling resistances [4]. Indeed, a clear increase in the load bearing capacity of welded
41 beams was observed when accounting for the flame-cuts. Complementary results are thus needed
42 to confirm these observations and to propose better design methods. The first objective of the
43 present paper is to conduct a large parametric study to evaluate the lateral-torsional buckling
44 resistance of welded I-section beams made of flame-cut flanges but also of hot-rolled flanges.

45 GMNIA-type calculations are thus performed using shell elements with the residual stress model
46 proposed by Lebastard et al. [4], focused on welded members made of flame-cut flanges and
47 based on experimental test results. These Geometrically and Materially Non-linear Analyses
48 account for the geometrical and material Imperfections of the member. The lateral-torsional
49 buckling behaviour of S275 and S355 uniform and tapered beams with a doubly or mono-
50 symmetric cross-section is investigated. The studied beams are subjected to end moments or a
51 transverse loading, uniformly distributed over the length or pointwise at mid-span. Additional
52 analyses are also performed considering similar welded beams but made of hot-rolled flanges,
53 using the residual stress model from prEurocode 3 Part 1-14 [5]. The numerical results show that

54 the current rules based on the buckling curve approach are adequate for welded beams made of
55 hot-rolled flanges for low-to-medium slenderness with a clear safety margin for increased
56 slenderness. For welded beams made of flame-cut flanges, the Eurocode rules are very
57 conservative, whatever the slenderness. These conclusions are drawn for all of the beam types
58 studied. A clear influence of the bending moment distribution on the buckling resistance is also
59 observed.

60 Partial factors are computed following the requirements of Eurocode 0 Annex D [6] and the
61 European RFCS project SAFEBRICKLE [7]. The values associated with the buckling curves
62 method confirm a significant over conservatism for welded beams made of flame-cut flanges.
63 Two enhanced methods are proposed for this type of beams. The first design method proposed
64 here makes use of one more favourable buckling curve and the second method, of an imperfection
65 factor defined per member and inversely proportional to the slenderness. The latter proposal also
66 accounts for the bending moment distribution in the determination of the buckling resistance. A
67 similar proposal is presented for welded beams made of hot-rolled flanges.

68 Besides, the predictions of the novel design method for computing the buckling resistance in prEN
69 1993-1-1 [1] developed by Taras ([8], [9]) are in good agreement with numerical results with a
70 small safety margin. However, this design method is limited to uniform doubly symmetric beams.
71 Other recent developments based on a consistent mechanical background have yielded design
72 methods adapted to tapered beams. Indeed, Marques et al. [10] proposed a method for tapered
73 beams depending on parameters calibrated using the results of a parametric study. In addition,
74 Tankova et al. [11] derived a *General formulation* adapted to uniform and tapered beams with a
75 doubly symmetric cross-section. This method relies on the second derivative of the elastic critical
76 buckling mode shape, the hand computation of which is generally excluded. Thus, finite element
77 analyses must be employed.

78 Since the novel design method prEN 1993-1-1 [1] is applicable solely in the case of uniform
79 doubly symmetric beams, its extension to tapered mono-symmetric beams is sought. Analytical
80 developments are realized using assumptions similar to those of Taras ([8], [9]). The resulting
81 method is analogous to the aforementioned one, with the introduction of a new parameter

- 82 accounting for the tapering and mono-symmetric design of the member. An imperfection factor
83 adapted to welded beams made of flame-cut flanges is suggested.

84 **2 DESIGN RULES FROM EUROCODE 3 AND**
 85 **PREUROCODE 3**

86 **2.1 Introduction**

87 The numerical results from Section 3 will be tested against the predictions of design rules for
 88 lateral-torsional buckling proposed in the project of Eurocode 3 Part 1-1 [1]. Two methods exist
 89 for uniform beams: the *General case*, presented in sub-Section 2.2, and a *new verification format*,
 90 described in 2.3. For non-uniform beams, Eurocode 3 Part 1-1 [1] requires the use of the *General*
 91 *Method* described in sub-Section 2.4. The design methods proposed in Section 4 are constructed
 92 within the framework of these methods while an extension of the new verification format is
 93 proposed.

94 **2.2 General case**

95 To assess the stability of a uniform member in bending, according to prEurocode 3 Part 1-1 [1],
 96 the following expression has to be verified:

$$\frac{M_{y,Ed}}{M_{b,Rd}} \leq 1.0 \quad (1)$$

97 with:

98 $M_{y,Ed}$: maximum design value of the bending moment about y - y (see Figure 1),

99 $M_{b,Rd}$: design value of the lateral-torsional buckling resistance obtained using:

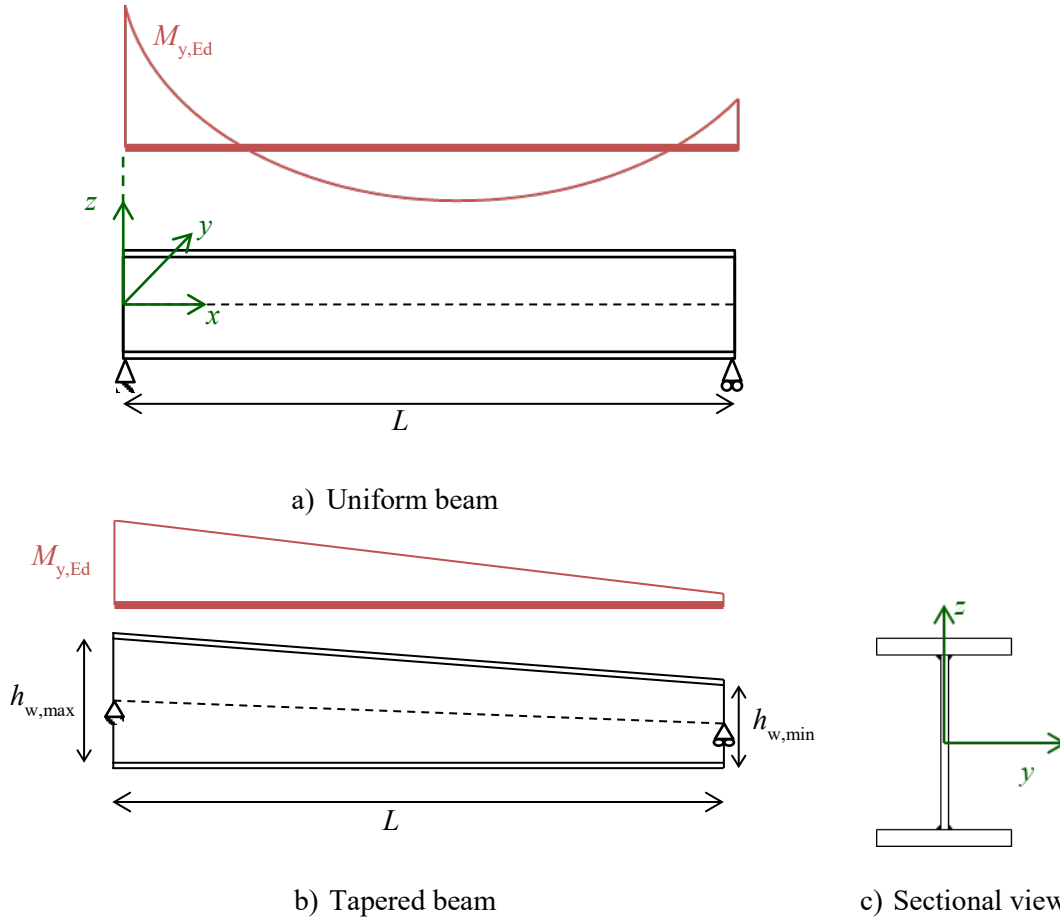
$$M_{b,Rd} = \chi_{LT} \frac{M_{y,Rk}}{\gamma_{M1}} \quad (2)$$

100 with:

101 $M_{y,Rk}$: characteristic value of the cross-section resistance against bending about y - y ,

102 χ_{LT} : reduction factor for lateral-torsional buckling,

103 γ_{M1} : partial factor for the resistance of members to instability.


Figure 1: Coordinate system and notations

104

105 To compute the reduction factor, one may use the “*General case*”, i.e. §6.3.2.2 of Eurocode 3 Part
 106 1-1 [2], which is based on the buckling curve approach. These buckling curves are founded on an
 107 extensive experimental study conducted on members in compression during the 1960s-1970s (see
 108 [12]-[14]). These studies yielded four buckling curves for I-section members in bending
 109 depending on the cross-section type and dimensions, the fabrication process, the steel grade and
 110 the buckling direction. Using the *General case* method, the reduction factor is given by:

$$\chi_{LT} = \frac{1}{\phi_{LT} + \sqrt{\phi_{LT}^2 - \bar{\lambda}_{LT}^2}} \leq 1.0 \quad (3)$$

$$\phi_{LT} = 0.5 \left[1 + \alpha_{LT} (\bar{\lambda}_{LT} - 0.2) + \bar{\lambda}_{LT}^2 \right] \quad (4)$$

111 with:

 112 α_{LT} : imperfection factor for lateral-torsional buckling (see Table 1),

113

Buckling curve	a	b	c	d
α_{LT}	0.21	0.34	0.49	0.76

114

Table 1: Imperfection factors

115

$\bar{\lambda}_{LT}$: normalized slenderness for lateral-torsional buckling:

$$\bar{\lambda}_{LT} = \sqrt{\frac{M_{y,Rk}}{M_{y,cr}}} \quad (5)$$

116

where $M_{y,cr}$ is the elastic critical lateral-torsional buckling bending moment.

117

The buckling curve selection for welded members, according to prEurocode 3 Part 1-1 [1], is

118

presented in Table 2. The two least favourable buckling curves are used for welded beams, but as

119

is common practice for steel buildings, the lateral-torsional buckling resistance of a welded beam

120

is computed using curve d , i.e. $h/b_{min} > 2.0$, where b_{min} is the minimum value between the widths

121

of the two flanges.

Limits	Buckling curve
$h/b_{min} \leq 2.0$	c
$h/b_{min} > 2.0$	d

122

Table 2: Buckling curve selection for welded members

123

A distinct design method from EN 1993 1-1 [2] makes use of a coefficient f to increase the lateral-

124

torsional buckling resistance accounting for the bending moment distribution. This design method

125

is not maintained in prEN 1993-1-1[1], but the French National Annex to EN 1993 1-1 [15] allows

126

for an increase in the reduction factor calculated with the *General case* depending on the bending

127

moment distribution using the coefficient f :

$$\chi_{LT, mod} = \frac{\chi_{LT}}{f} \leq 1.0 \quad (6)$$

$$f = 1 - 0.5(1 - k_c) \left[1 - 2.0(\bar{\lambda}_{LT} - 0.8)^2 \right] \leq 1.0 \quad (7)$$

128

where the correction factor k_c is given in Table 3 for usual load cases.

129


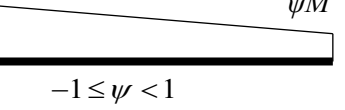

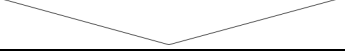
	Moment distribution	k_c	f_M
130		1.0	1.0
131		$\frac{1}{1.33 - 0.33\psi}$	$1.25 - 0.1\psi - 0.15\psi^2$
132		0.94	1.05
133		0.86	1.10

 Table 3: Factors k_c and f_M

2.3 New verification format

As an alternative to the *General case*, prEN 1993-1-1 [1] proposes a new design method to compute the reduction factor χ_{LT} . Based on consistent analytical developments realized by Taras ([8], [9]), this “*new verification format*” is proposed for the use of uniform doubly symmetric beams resting on fork supports at both ends:

$$\chi_{LT} = \frac{f_M}{\phi_{LT} + \sqrt{\phi_{LT}^2 - f_M \bar{\lambda}_{LT}^2}} \leq 1.0 \quad (8)$$

$$\phi_{LT} = 0.5 \left[1 + f_M \left(\left(\frac{\bar{\lambda}_{LT}}{\bar{\lambda}_z} \right)^2 \alpha_{LT} (\bar{\lambda}_z - 0.2) + \bar{\lambda}_{LT}^2 \right) \right] \quad (9)$$

where the factor f_M depends on the bending moment distribution and is given in Table 3 for simple bending moment diagrams.

Different values of the imperfection factor α_{LT} are defined in prEN 1993-1-1 [1] for welded beams depending on the flange thickness (see Table 4). In common practice for steel buildings, the flange thickness of welded members is less than or equal to 40 mm; the first line of Table 4 therefore generally applies.

Limits	α_{LT}
$t_f \leq 40$ mm	$0.21 \sqrt{\frac{W_{el,y}}{W_{el,z}}} \leq 0.64$
$t_f > 40$ mm	$0.25 \sqrt{\frac{W_{el,y}}{W_{el,z}}} \leq 0.76$

Table 4: Buckling curve selection for welded members

2.4 General Method

143

144 According to Eurocode 3 Part 1-1 [2], the stability verification of a non-uniform member in
145 bending can be performed using the *General Method* which requires the following criterion to be
146 verified:

$$\frac{\chi_{LT}\alpha_{ult,k}}{\gamma_{M1}} \geq 1.0 \quad (10)$$

147 where the minimum amplifier of the design loads reaching the characteristic resistance of the most
148 critical cross-section of the beam, $\alpha_{ult,k}$, is obtained using:

$$\alpha_{ult,k}(x) = \frac{M_{y,Rk}(x)}{M_{y,Ed}} \quad (11)$$

149 The reduction factor χ_{LT} is computed for the normalized slenderness given by:

$$\bar{\lambda}_{LT} = \sqrt{\frac{\alpha_{ult,k}}{\alpha_{cr,op}}} \quad (12)$$

150 where $\alpha_{cr,op}$ is the minimum amplifier of the design loads to trigger the elastic lateral-torsional
151 buckling of the beam.

152 The predictions of both the *General case* and the *new verification format* will be compared against
153 GMNIA results obtained for uniform beams using the numerical model described in the next
154 Section. For tapered beams, the numerical results will be compared against predictions of the
155 *General Method* used along with the *General case*.

156

157

3 FINITE ELEMENT ANALYSES

158

3.1 Presentation of the finite elements model

159

The numerical model is developed using the ANSYS v.2020 software package by means of four-

160

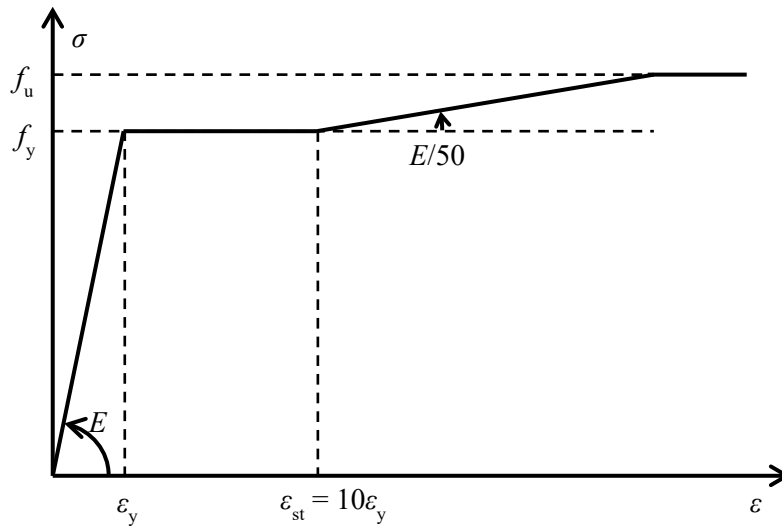
noded shell finite elements (SHELL 181). The multilinear material law depicted in Figure 2 is

161

considered with an elastic regime characterized by a Young's modulus of $E = 210\,000$ MPa and

162

a Poisson's ratio of $\nu = 0.3$.



163

164

Figure 2: Material law

165

Residual stress models for welded members made of hot-rolled flanges (see Figure 3a)) or made

166

of flame-cut flanges (see Figure 3b)) are implemented. The model employed for welded beams

167

with hot-rolled flanges corresponds to that prescribed by prEurocode 3 Part 1-14 [5] based on the

168

ECCS model [16]. The model for flame-cut flanges proposed by Lebastard et al. [4] depends on

169

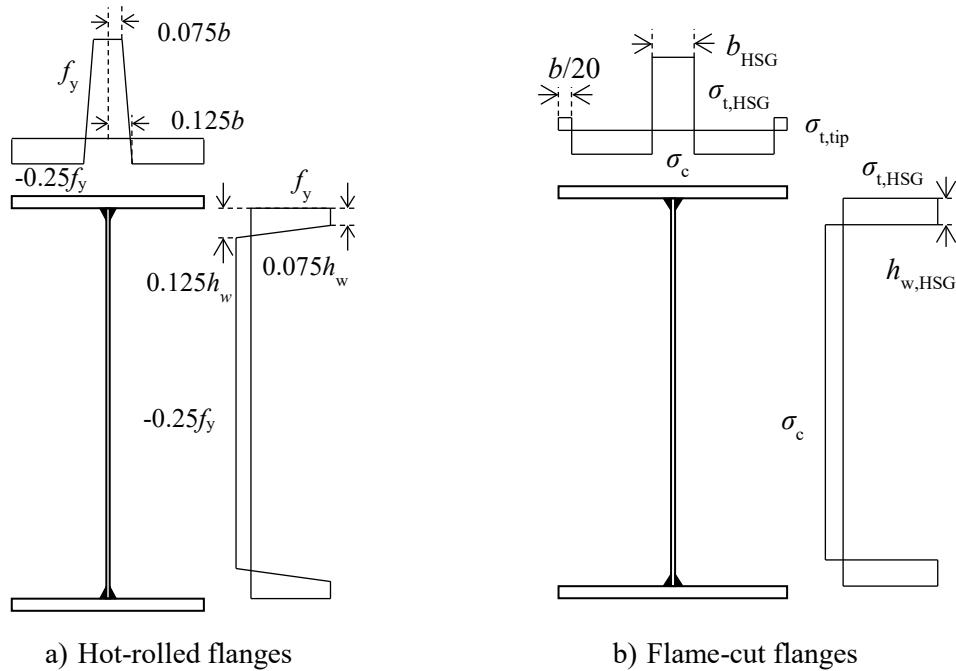
the following parameters:

$$\sigma_c = -f_y \left(0.25 - 0.005 \frac{b}{t_f} \right) \leq -0.14 f_y \quad (13)$$

$$\sigma_{t,tip} = f_y \left(0.70 - 0.35 \frac{h_t}{b} \right) \geq 0.03 f_y \quad (14)$$

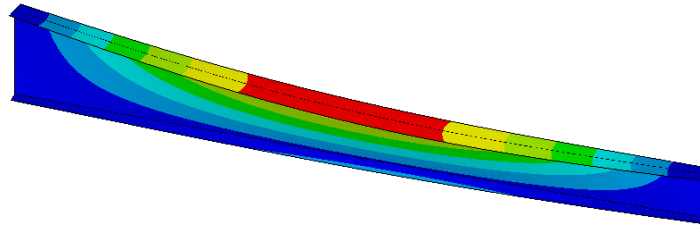
$$b_{HSG} = b \left(0.1 + 0.036 \frac{h_t}{b} \right) \quad (15)$$

170 Furthermore, geometrical imperfections are introduced as recommended by Annex C of Eurocode
 171 3 Part 1-5 [17] and prEurocode 3 Part 1-14 [5]. A global imperfection is enforced using the
 172 buckling mode shape resulting from a Linear Bifurcation Analysis (LBA), as presented in Figure
 173 4a) and suggested by Couto et al. [18]. Local imperfections are also introduced using sine waves
 174 having similar half-periods in all plates, as recommended by Gérard et al. [19] and illustrated in
 175 Figure 4b).



176 **Figure 3: Residual stresses in welded members**

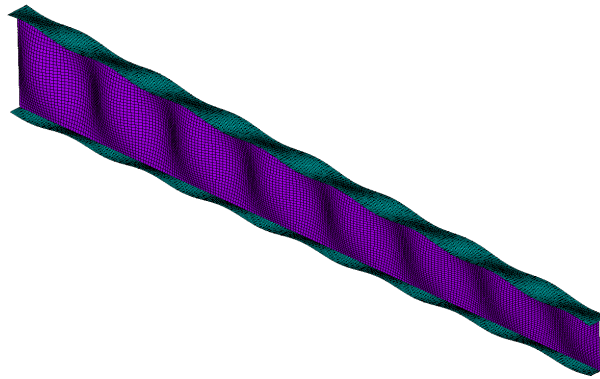
177 The amplitude of the global imperfection is set to $L/1000$, with L being the distance between the
 178 beam ends, as recommended by Boissonnade et al. [20] and Couto et al. [18]. The amplitudes of
 179 the local imperfections are $h_w/200$ in the web and $b/200$ in the flanges. These amplitudes are
 180 recommended by Eurocode 3 Part 1-5 [17] and prEurocode 3 Part 1-14 [5]. Both types of
 181 geometrical imperfections are integrated simultaneously, the magnitudes of the local
 182 imperfections are then reduced to 70% of their original values as prescribed by Eurocode 3 ([5],
 183 [17]).



184

185

a) Global imperfection



186

187

b) Local imperfections

188

Figure 4: Shape of geometrical imperfections

189 Fork support conditions are implemented at both ends by fully preventing vertical and lateral
190 displacements as well as twist rotation. Longitudinal displacement is constrained at one end to
191 prevent rigid body motion. The numerical model was previously validated by comparison against
192 experimental tests [4]. To that end, experimental results of the tests campaigns presented by
193 Lebastard et al. [4], Tankova [21], Schaper et al. [22] and Ji et al. [23] for welded members with
194 flame-cut flanges were employed.

195

3.2 *Scope of the study*

196

197

198

199

200

201

202

203

Using the numerical model previously described and validated against experimental results, an
extensive parametric study is conducted. A total of 1129 GMNIA-type computations are
performed for welded beams. The vast majority of the beams studied had flame-cut flanges.
Linear bending moment distributions are investigated with a ratio between end moments ψ of -1;
-0.5; 0; 0.5 or 1 as well as with transverse loadings. Beams are studied subjected to a mid-span
pointwise transverse force or a load uniformly distributed over the length, applied either at the
cross-section shear centre or at the centroid of the compressive or tensile flange. Normalized
slenderness for lateral-torsional buckling is up to 3. The following cross-section types are studied:

204 ➤ Uniform and doubly symmetric;

205 ➤ Uniform and mono-symmetric;

206 ➤ Web-tapered and doubly symmetric, or

207 ➤ Web-tapered and mono-symmetric.

208 The dimensions of the uniform and tapered beams studied here are presented in Table 5 and Table
 209 6, respectively, based on the cross-section dimensions shown in Figure 5. The parametric study
 210 focussed on steel grades of S355 and S275. A single flange is inclined in tapered beams. For
 211 mono-symmetric beams, the subscript “c” is assigned to the compressive flange under positive
 212 bending moment and “t” to the tensile flange.

213 In addition, 154 GMNIA computations are performed on uniform doubly symmetric welded
 214 beams made of hot-rolled flanges. The dimensions are presented in Table 5; analogous beams are
 215 also studied but with flame-cut flanges.

Linear bending moment distribution		
Doubly symmetric beams	Mono-symmetric beams	Transverse loading
$h_w \times b \times t_w \times t_f$	$h_w \times b_c(b_t) \times t_w \times t_{f,c}(t_{f,t})$	
1000×200×8×25	1000×350(200)×8×25(25)_r	
1000×300×8×25	900×250(250)×6×30(18)_r	800×200×10×15
900×250×6×18	800×350(200)×6×20(20)_r	500×150×15×20
800×200×6×20*	800×200(200)×6×25(15)	500×150(100)×10×20(10)_r
600×200×6×16*	600×300(200)×6×25(16)_r	400×160×8×14
450×230×5×12*	600×250(250)×5×20(15)	250×200×12×14
300×170×5×12*	450×230(230)×5×24(12)_r	
	300×170(170)×5×20(12)_r	

*: Uniform doubly symmetric beams studied with hot-rolled flanges.

_r: Mono-symmetric beams also studied with the largest flange in tension.

216 **Table 5: Uniform welded beams studied (mm)**

217 The dimensions are chosen in line with common practice for steel buildings. Indeed, the beams
 218 depths range between 250 and 1000 mm with thickness of 5 to 10 mm. The flange widths vary
 219 between 100 and 350 mm, most of them are Class 1 or 2 under uniform compression. Mono-
 220 symmetric beams are characterized by ratios between the flange widths of up to 1.75 and ratios

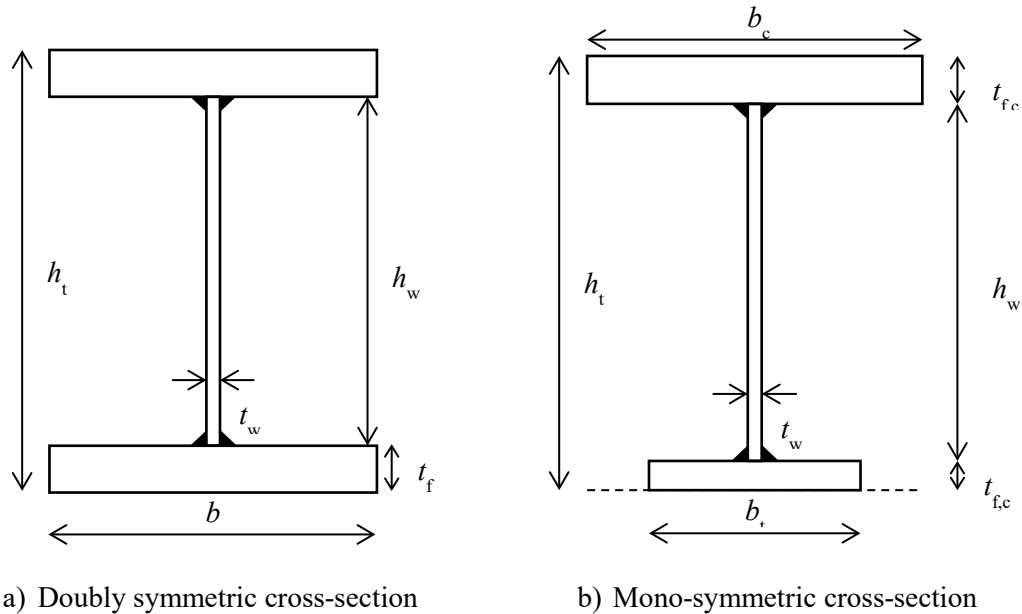
221 between the flange thickness of up to 2. The majority of mono-symmetric beams are studied with
 222 the largest flange in compression under a positive bending moment, corresponding to common
 223 practice. However, some beams are analysed with the largest flange in tension. All the studied
 224 beams subjected to a transverse loading are uniform, with either a doubly or a mono-symmetric
 225 cross-section.

Doubly symmetric beams	Mono-symmetric beams
$h_{w,max}(h_{w,min}) \times b \times t_w \times t_f$	$h_{w,max}(h_{w,min}) \times b_c(b_t) \times t_w \times t_{f,c}(t_{f,t})$
1000(500) × 200 × 8 × 25	1000(350) × 350(200) × 8 × 25(25)_r
900(300) × 250 × 10 × 25	800(400) × 200(200) × 6 × 25(15)_r
800(400) × 200 × 6 × 20	600(400) × 300(200) × 6 × 25(16)
750(450) × 230 × 6 × 20	634(230) × 230(230) × 5 × 24(12)
600(400) × 200 × 6 × 16	

_r: Mono-symmetric beams also studied with the largest flange in tension.

226

Table 6: Tapered welded beams studied (mm)



227

Figure 5: Cross-sectional dimensions

3.3 Results of the parametric study

3.3.1 Introduction

The numerical results obtained from this parametric study are confronted to the buckling curves of EN 1993-1-1 [2] for lateral-torsional buckling. In addition, the safety and accuracy of the Eurocode design rules for welded members in bending are assessed by computing partial factors according to the prescriptions of Annex D of EN 1990 [6] and the recommendations of the RFCS European project SAFEFRICITILE [7]. The prescriptions of Annex D remain similar in prEN 1990 [24]. The statistical data used for the input variables correspond to those provided in Annex E from prEN 1993-1-1 [1]. A unique value of 1.0 is the target for the partial factor, in agreement with common practice. Partial factors associated with the European rules are computed first and will then be used to define satisfactory safety levels. The results are presented for various subsets, as recommended in [7], but also for the full set of results. The latter cannot be used to evaluate the safety level but may indicate a lack of accuracy or a variable sensitivity of the method.

3.3.2 Uniform beams under end moments

Numerical analyses are carried out for two sets of bending moments for uniform beams:

- $M_{y,cr,LBA}$: elastic critical bending moment;
- $M_{y,ult,GMNIA}$: ultimate bending moment.

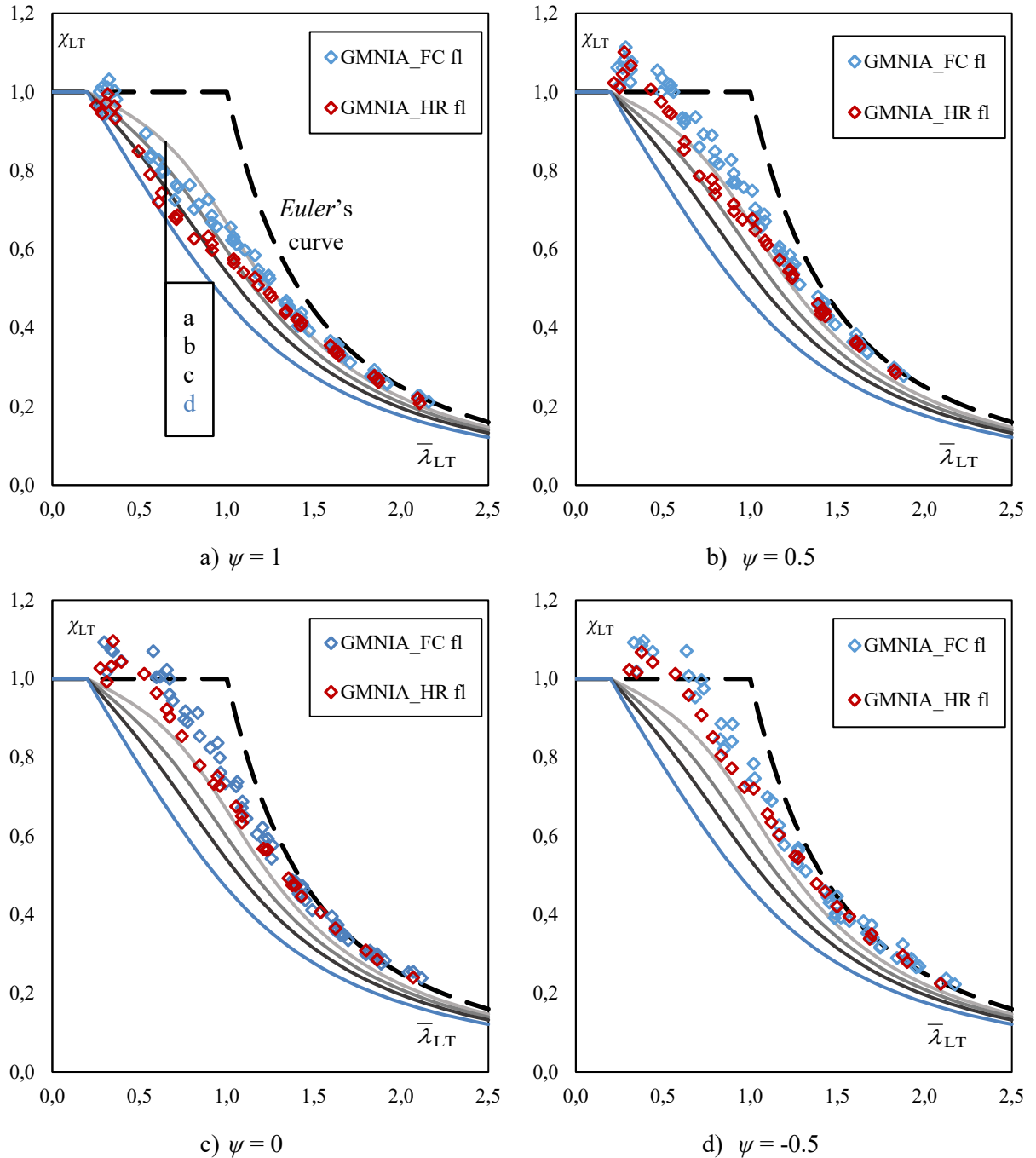
These values are used along with the characteristic cross-section resistance against bending about the major axis $M_{y,Rk}$ following the prescriptions of EN 1993-1-1 [2] and EN 1993-1-5 [17] to calculate the normalized slenderness:

$$\bar{\lambda}_{LT} = \sqrt{\frac{M_{y,Rk}}{M_{y,cr,LBA}}} \quad (16)$$

and the reduction factor:

$$\chi_{LT,GMNIA} = \frac{M_{y,ult,GMNIA}}{M_{y,Rk}} \quad (17)$$

249 The numerical reduction factors obtained are plotted against the normalized slenderness in Figure
 250 6 for uniform doubly symmetric beams with buckling curves *a* to *d*. It is worth recalling that the
 251 *General case* ([1], [2]) commonly requires the use of buckling curve *d* for welded beams.



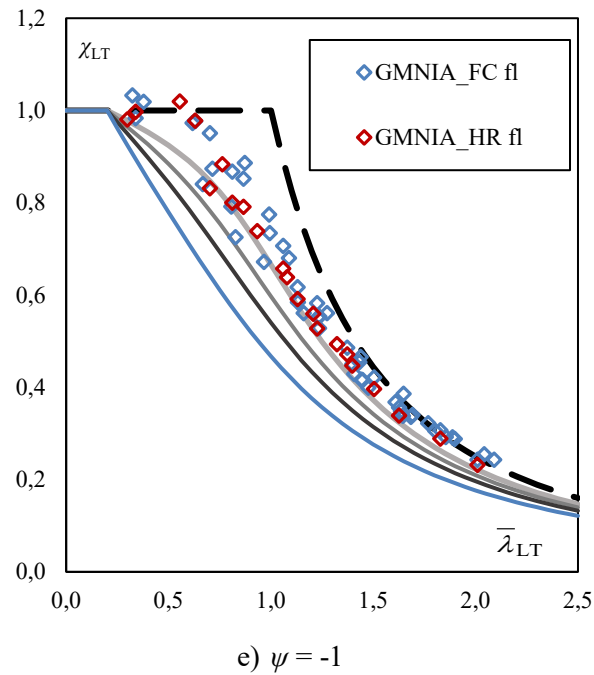


Figure 6: Numerical results for uniform doubly symmetric beams

252
 253 Figure 6 shows that the numerical results for welded beams made of flame-cut flanges are always
 254 above buckling curve *c*. The lowest results are obtained for a uniform bending moment diagram
 255 and are found between curves *a* and *c* in the low-to-intermediate slenderness range (up to
 256 approximately 1). For increased slenderness, the numerical results are closer to *Euler's* curve. For
 257 the other moment distributions, all numerical results considering the flame-cuts lie above buckling
 258 curve *a*, except for a few cases in Figure 6e) corresponding to $\psi = -1$. In this case, internal shear
 259 forces are significant in the low-to-medium slenderness range, which reduces the ultimate bending
 260 moment. The resulting buckling mode may feature web buckling owing to shear.
 261 Besides, a clear impact of the flange fabrication process is observed. Ultimate bending moments
 262 for welded beams made of hot-rolled flanges are lower than those accounting for flame-cut
 263 flanges. This effect is diminished as ψ decreases and the slenderness increases. In the least
 264 favourable case, i.e. the constant moment diagram, the numerical results for welded beams with
 265 hot-rolled flanges lie between buckling curves *c* and *d* in the low slenderness range while moving
 266 closer to *Euler's* curve as the slenderness increases.
 267 The numerical results obtained for uniform mono-symmetric beams are shown in Figure 7. The
 268 results obtained for a constant bending moment are presented in Figure 7a) while Figure 7b)

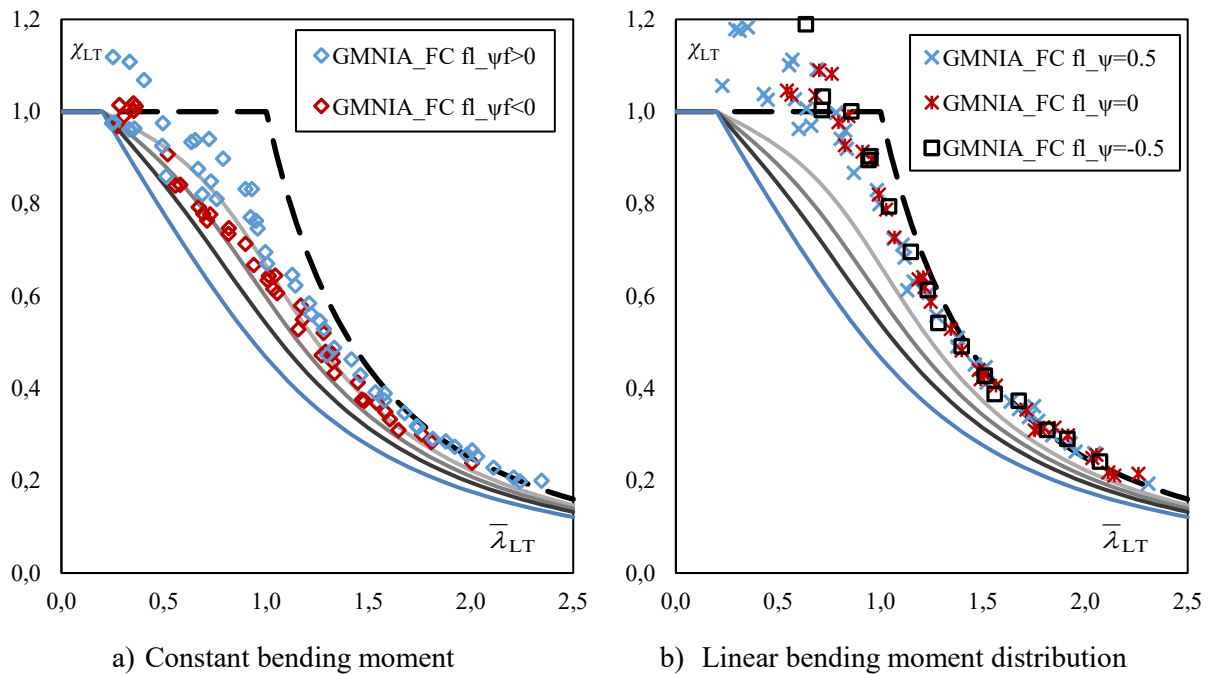
269 shows those for a linear bending moment distribution. For a constant bending moment
 270 distribution, two types of loading are applied, depending on the sign of:

$$\psi_f = \frac{I_{fc} - I_{ft}}{I_{fc} + I_{ft}} \quad (18)$$

271 where I_{fc} and I_{ft} are the second moments of area about the z-axis of the compressive and tensile
 272 flanges, respectively.

273 In common practice $\psi_f > 0$, i.e. the larger flange is in compression (under a positive moment). For
 274 a linear moment distribution, the larger flange is thus in compression at the cross-section end
 275 subjected to the greatest magnitude of the bending moment diagram.

276 Figure 7a) shows scattered results when the largest flange is compressed while the scatter is
 277 reduced if the smallest flange is in compression. The latter case yields the lowest results. Whatever
 278 the compressive flange type, the reduction factors lie above buckling curve *c* and tend towards
 279 *Euler's* curve as the slenderness increases. For the linear bending moment diagram, the results
 280 are above buckling curve *a*, showing a very limited influence of imperfections on the buckling
 281 resistance.



282 **Figure 7: Numerical results for uniform mono-symmetric beams**

283 For uniform doubly and mono-symmetric beams, Figure 6 and Figure 7 highlight that the use of
 284 buckling curve d , as prescribed by the *General case* from Eurocode 3 and prEurocode 3 Part 1-1
 285 ([1], [2]) in most cases, is overly conservative for welded beams made of flame-cut flanges. Both
 286 figures also show an influence of the bending moment distribution on the buckling resistance.

287 3.3.2.1 Assessment of the General case from EN 1993-1-1 [2]

288 • **Welded beams made of hot-rolled flanges**

289 The partial factors associated with the design methods for welded members in bending are
 290 determined for:

- 291 • The low slenderness range: $\bar{\lambda}_{LT} \leq 0.8$;
- 292 • The intermediate slenderness range: $0.8 < \bar{\lambda}_{LT} \leq 1.5$;
- 293 • The high slenderness range: $1.5 < \bar{\lambda}_{LT}$.

294 The partial factors associated with the *General case* are given in Table 7 for uniform doubly
 295 symmetric welded beams made of hot-rolled flanges. The partial factor is close to unity in the low
 296 slenderness range, being equal to 1.03. In the intermediate and high slenderness ranges, partial
 297 factors are clearly less than 1.0: the current design method is very conservative for these
 298 slenderness ranges. An enhanced design method is thus proposed in sub-Section 4.1.2.

Slenderness range	n	γ_{M1}
$\bar{\lambda}_{LT} \leq 0.8$	52	1.028
$0.8 < \bar{\lambda}_{LT} \leq 1.5$	72	0.904
$1.5 < \bar{\lambda}_{LT}$	30	0.866
All ranges	154	1.046

299 **Table 7: Partial factors of the *General case* for beams with hot-rolled flanges**

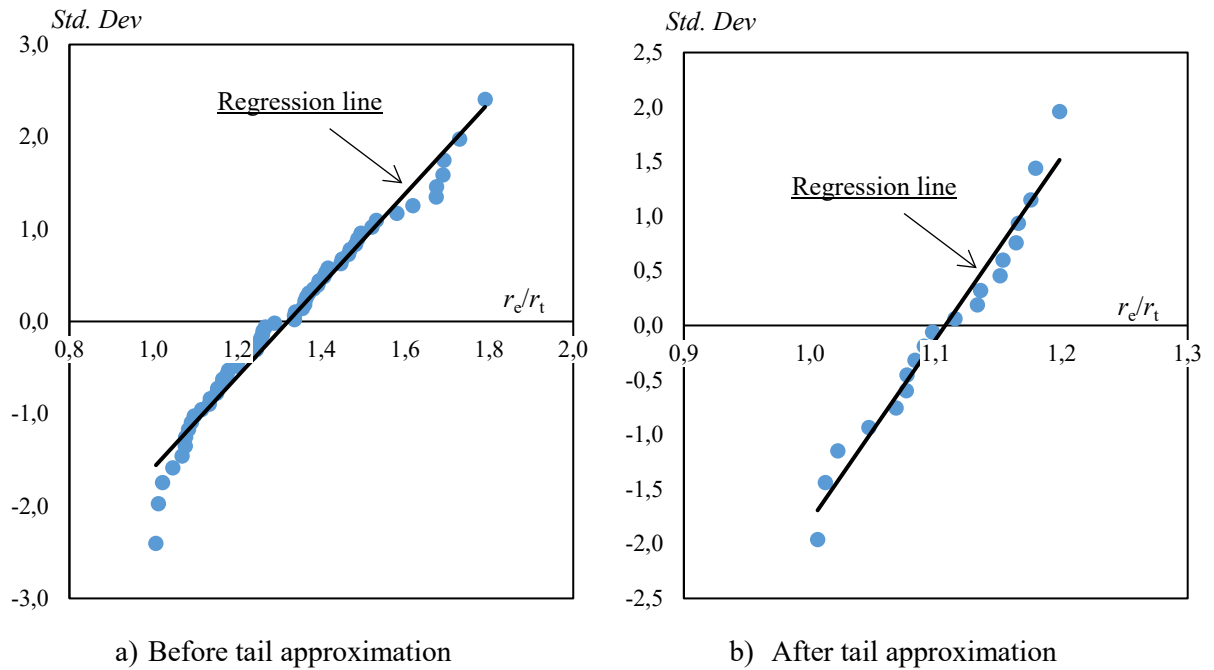
300 • **Welded beams made of flame-cut flanges**

301 The partial factors associated with the *General case* for uniform welded beams made of flame-
 302 cut flanges are presented in Table 8. Very low values are obtained for medium and high
 303 slenderness (between 0.81 and 0.85), which characterize a significant over-conservatism of this
 304 design method for both cross-section types.

Slenderness range	Doubly symmetric		Mono-symmetric	
	n	γ_{M1}	n	γ_{M1}
$\bar{\lambda}_{LT} \leq 0.8$	107	1.003	62	<u>1.108</u>
$0.8 < \bar{\lambda}_{LT} \leq 1.5$	180	0.807	77	0.821
$1.5 < \bar{\lambda}_{LT}$	100	0.809	57	0.848
All ranges	387	0.982	196	1.001

Table 8: Partial factors of the *General case* for beams with flame-cut flanges

305
306 For the low slenderness range, a value close to unity is found for doubly symmetric beams while
307 1.11 is obtained for mono-symmetric beams despite the absence of unsafe result. This discrepancy
308 is due to the very scattered results (see Figure 7) with some extremely safe results. The quantile
309 plot associated with the *General case* for mono-symmetric beams with a low slenderness is
310 displayed in Figure 8a). The applied procedure relies on the assumption of a (log-) normal
311 distribution of the results. Quantile plots should therefore exhibit individual results very close to
312 the regression line of the values studied. However, Figure 8a) shows that the regression line lies
313 away from the smallest ratio r_e/r_t due to overly conservative results.
314 A “tail approximation” is therefore performed, which consists in neglecting the most conservative
315 results. The distribution of the remaining significant results should then be in line with a normal
316 distribution, as described in the SAFEBRICKTILE project [7]. Consequently, it is decided to
317 remove all specimens for which r_e/r_t is greater than 1.20, yielding the quantile plot of Figure 8b).
318 Using the tail approximation reduces the partial factor from 1.11 to 1.02 which is acceptable.



319 **Figure 8: Quantile plot of the *General case* – uniform mono-symmetric beams (low**
 320 **slenderness)**

321 The previous results obtained using the *General case* are not well suited for welded beams made
 322 of flame-cut flanges. This design method is excessively conservative for most members used in
 323 practice. In addition, the precision of this method strongly depends on the slenderness of the beam.
 324 Improved reduction factors, adapted to welded beams made of flame-cut flanges are therefore
 325 proposed in sub-Section 4.1.1.

326 3.3.2.2 Assessment of the new verification format from prEN 1993-1-1 [1]

- 327 • **Welded beams made of hot-rolled flanges**

328 In addition to the *General case*, the safety assessment of the *new verification format* of
 329 prEurocode 3 Part 1-1 [1] is investigated. The corresponding values of γ_{M1} are given in Table 9
 330 for uniform doubly symmetric beams with hot-rolled flanges.

Slenderness range	n	γ_{M1}
$\bar{\lambda}_{LT} \leq 0.8$	52	0.975
$0.8 < \bar{\lambda}_{LT} \leq 1.5$	72	1.021
$1.5 < \bar{\lambda}_{LT}$	30	0.989
All ranges	154	1.080

332 **Table 9: Partial factors of the *new verification format* for beams with hot-rolled flanges**

333 Within the three slenderness ranges, the γ_{M1} -values are very close to unity. The values are between
 334 0.98 and 1.02. This design method is well suited for welded uniform doubly symmetric I-section
 335 beams made of hot-rolled flanges.

336 • **Welded beams made of flame-cut flanges**

337 The partial factors associated with the *new verification format* are presented in Table 10 for
 338 welded beams with flame-cut flanges. For all ranges of slenderness, the partial factors are between
 339 0.95 and 0.99, showing a good accuracy of the design method. Slightly more favourable
 340 imperfection factors are proposed in Section 4.2.2.

Cross-section type	Slenderness range	n	γ_{M1}
Doubly symmetric	$\bar{\lambda}_{LT} \leq 0.8$	107	0.947
	$0.8 < \bar{\lambda}_{LT} \leq 1.5$	180	0.987
	$1.5 < \bar{\lambda}_{LT}$	100	0.991
	All ranges	387	1.044

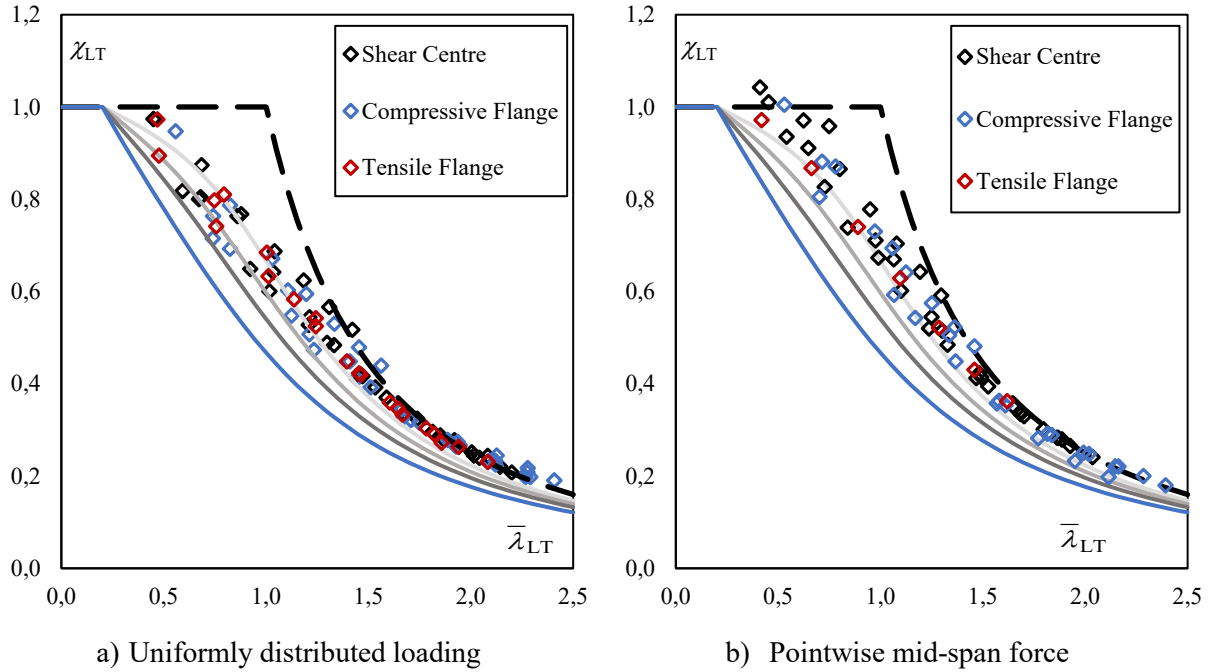
341 **Table 10: Partial factors of the *new verification format* for beams with flame-cut flanges**

342 This design method is applicable in the case of uniform and doubly symmetric beams only. The
 343 extension of its scope to cover tapered and/or mono-symmetric beams is therefore addressed in
 344 sub-Section 4.2.1.

345 **3.3.3 *Uniform beams under transverse loading***

346 The numerical reduction factors (see Eq. (17)) obtained for uniform doubly and mono-symmetric
 347 beams under a transverse loading are presented in Figure 9. The results lie between buckling
 348 curves c and b in the least favourable cases for uniform loading, and between curves b and a for
 349 a pointwise force. The lowest values are found for low-to-intermediate slenderness. Again, the
 350 numerical results move closer to *Euler's* curve as the slenderness increases. Besides, Figure 9

351 illustrates the effect of the bending moment distribution on the results. Indeed, the reduction
 352 factors obtained for a pointwise mid-span force are somewhat greater than those obtained for a
 353 uniformly distributed loading, especially for low and intermediate slenderness.



354 **Figure 9: Numerical results for uniform beams under transverse loading**

355 3.3.3.1 Assessment of the General case from EN 1993-1-1 [2]

356 The partial factors associated with the *General case* are computed for the set of welded beams
 357 studied with flame-cut flanges under transverse loading. The results are presented in Table 11
 358 with modified slenderness range, the boundary between low and medium slenderness being set to
 359 1 to better suit the study cases. Since the partial factors are significantly lower than unity, ranging
 360 between 0.76 and 0.89, this design method is found to be exceedingly conservative.

Slenderness range	n	γ_{M1}
$\bar{\lambda}_{LT} \leq 1$	40	0.898
$1 < \bar{\lambda}_{LT} \leq 1.5$	55	0.772
$1.5 < \bar{\lambda}_{LT}$	73	0.757
All ranges	168	0.867

361 **Table 11: Partial factors of the *General case* for beams with flame-cut flanges under**
 362 **transverse loading**

363 3.3.3.2 Assessment of the new verification format from prEN 1993-1-1 [1]

364 The partial factors associated with the *new verification format* are determined for the welded
 365 beams with flame-cut flanges under transverse loading that present a doubly symmetric cross-
 366 section. Indeed, mono-symmetric cross-sections are not within the scope of this design method.
 367 The results, presented in Table 12, are close to unity, being between 0.96 and 1.03. This design
 368 method is well suited for the studied beams.

Slenderness range	n	γ_{M1}
$\bar{\lambda}_{LT} \leq 1$	30	1.034
$1 < \bar{\lambda}_{LT} \leq 1.5$	35	1.029
$1.5 < \bar{\lambda}_{LT}$	33	0.956
All ranges	98	1.078

369 **Table 12: Partial factors of the *new verification format* for beams with flame-cut flanges**
 370 **under transverse loading**

371 3.3.4 Tapered beams

372 In the case of non-uniform beams, the following two sets of load amplifiers result from the
 373 numerical analyses:

- 374 • $\alpha_{cr,LBA}$: elastic critical load amplifier for lateral-torsional buckling;
- 375 • $\alpha_{op,GMNIA}$: ultimate load amplifier.

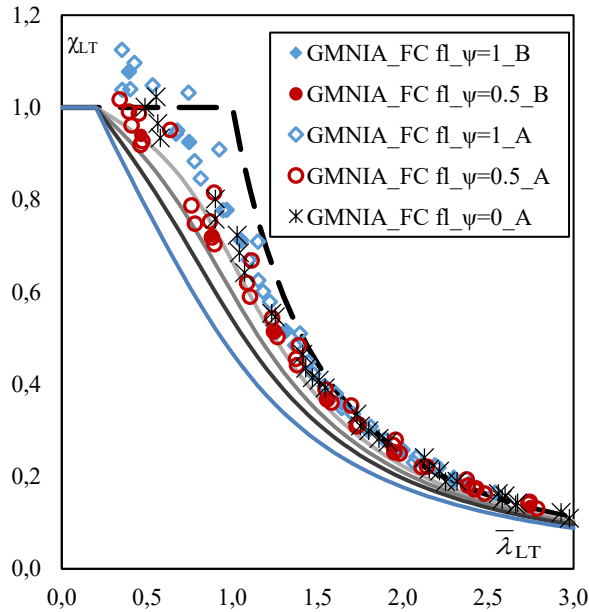
376 The minimum value of $\alpha_{ult,k}$, evaluated analytically using Eq. (11), at several cross-sections along
 377 the member is used with $\alpha_{cr,LBA}$ and $\alpha_{op,GMNIA}$ to compute:

$$\bar{\lambda}_{LT} = \sqrt{\frac{\alpha_{ult,k}}{\alpha_{cr,LBA}}} \quad (19)$$

$$\chi_{LT,GMNIA} = \frac{\alpha_{op,GMNIA}}{\alpha_{ult,k}} \quad (20)$$

378 The numerical results are presented in Figure 10 for doubly symmetric tapered beams. The
 379 compressive and tensile flanges are inclined for types *A* and *B*, respectively. Similar results are
 380 obtained for both types of beams that lie above buckling curve *b*. In the case of a constant or

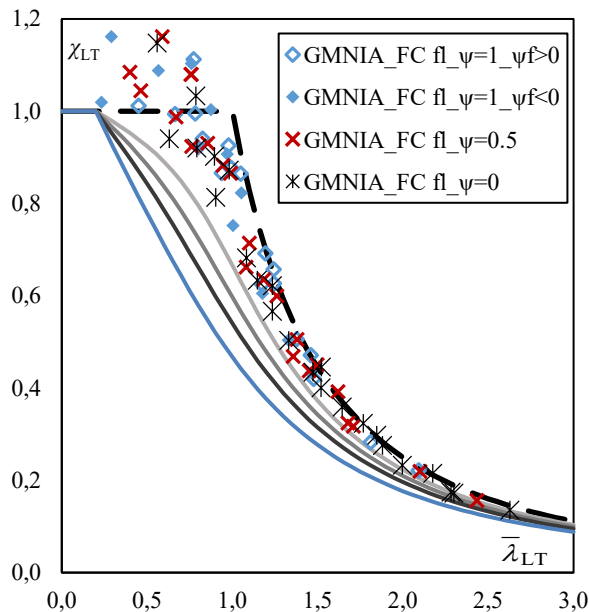
381 triangular moment distribution, all numerical results are above curve *a*. Again, the results are
 382 closer to *Euler's* curve as the slenderness increases.



383

384 **Figure 10: Numerical results for tapered doubly symmetric beams**

385 Figure 11 presents the numerical results obtained for tapered mono-symmetric beams, where only
 386 the compressive flange is inclined. All results lie above buckling curve *a* and move closer to
 387 *Euler's* curve as the slenderness increases. For the constant bending moment, the results are
 388 slightly greater when $\psi_f > 0$ than when $\psi_f < 0$.



389

390 **Figure 11: Numerical results for tapered mono-symmetric beams**

391 Both Figure 10 and Figure 11 show that the use of buckling curve d as generally prescribed by
 392 the European code is exceedingly conservative for welded beams made of flame-cut flanges,
 393 similar to the case of uniform beams. The partial factors associated with Eurocode 3 rules for
 394 welded beams are then computed.

395 • **Assessment of the *General Method* of EN 1993-1-1 [2]**

396 The stability of non-uniform members can be assessed according to EN 1993-1-1 [2] using the
 397 *General Method* (see §2.4), which requires computation of reduction factor χ_{LT} . Since the *new*
 398 *verification format* does not apply to non-uniform beams, the reduction factor is computed using
 399 the *General case*.

400 The partial factors for tapered welded beams made of flame-cut flanges associated with the
 401 *General Method* are computed for the low, intermediate and high slenderness ranges. The
 402 transition between the intermediate and high slenderness ranges for tapered mono-symmetric
 403 beams is set to 1.25 instead of 1.5 owing to the limited number of results for members with a
 404 normalized slenderness greater than 1.5.

405 The resulting partial factors are very low for the intermediate and high slenderness ranges for both
 406 cross-section types, with values between 0.73 and 0.85. A safety margin is also noted for the low
 407 slenderness range. The γ_{M1} values characterize an excessively conservative design method. This
 408 method is not appropriate for welded beams made of flame-cut flanges. Reduction factors adapted
 409 to the flame-cuts are proposed in Section 4. Since the scope of the *new verification format* of
 410 prEurocode 3 Part 1-1 [1] is restricted to uniform beams with a doubly symmetric cross-section,
 411 its extension to tapered and/or mono-symmetric beams, which are commonly used, is also
 412 proposed in Section 4.

Doubly symmetric			Mono-symmetric		
Slenderness range	n	γ_{M1}	Slenderness range	n	γ_{M1}
$\bar{\lambda}_{LT} \leq 0.8$	26	0.977	$\bar{\lambda}_{LT} \leq 0.8$	38	0.911
$0.8 < \bar{\lambda}_{LT} \leq 1.5$	42	0.790	$0.8 < \bar{\lambda}_{LT} \leq 1.25$	28	0.728
$1.5 < \bar{\lambda}_{LT}$	61	0.850	$1.25 < \bar{\lambda}_{LT}$	29	0.825
All ranges	129	0.913	All ranges	95	0.850

413 **Table 13: Partial factors of the *General Method* for tapered beams**

3.4 Summary

414 A numerical parametric study was carried out as depicted in sub-Section 3.2 based on the finite
415 shell elements model presented in sub-Section 3.1. The parametric study comprised 1129 cases
416 of welded beams varying in:

- 418 • Flange type: hot-rolled or flame-cut;
- 419 • Cross-section shape: doubly or mono-symmetric;
- 420 • Member shape: uniform or tapered;
- 421 • Loading conditions: end moments or transverse loading, applied pointwise at mid-span
422 or uniformly distributed.

423 The numerical results highlighted the decreasing effect of the member imperfections on the
424 ultimate bending moment as the slenderness increases. A visible impact of the bending moment
425 distribution on the bending moment resistance was also noted. Besides, numerical results were
426 employed to compute the γ_{M1} -factors associated with Eurocode 3 and prEurocode 3 Part 1-1 ([1],
427 [2]) rules for welded beams following the requirements of EN 1990 Annex D [6] and the
428 recommendations of the RFCS European project SAFEBRICKTILE [7].

429 For welded beams with flame-cut flanges, the partial factors associated with the *General case*
430 were significantly lower than unity, in particular in the medium and high slenderness ranges,
431 characterizing an exceedingly conservative design method. The partial factors related to the *new*
432 *verification format* were closer to 1, but this design method applies to uniform doubly symmetric
433 beams only. In the case of welded beams with hot-rolled flanges, partial factors associated with
434 the *General case* were clearly lower than unity for slender members while the values
435 characterizing the *new verification format* proved to be satisfactory. The shortcomings of the
436 current design rules will be addressed by proposing enhanced design methods for welded beams
437 in the upcoming Section 4

438 4 DESIGN METHODS

439 4.1 *Adaptation of the General case*

440 4.1.1 Welded beams made of flame-cut flanges

441 4.1.1.1 Uniform beams

442 Two proposals are adapted from the current and revised *General case* from Eurocode 3 and
 443 prEurocode 3 Part 1-1 ([1], [2]) for welded beams made of flame-cut flanges. The first proposal
 444 consists in computing the design value of the lateral-torsional buckling resistance $M_{b,Rd}$ using
 445 expressions (2) – (4) but with the imperfection factor corresponding to buckling curve c for
 446 welded beams made of flame-cut flanges in steel buildings, i.e.:

$$\alpha_{LT} = 0.49 \quad (21)$$

447 *Proposition 1* is similar to that of Thiébaud [27] for welded bridge girders with flame-cut flanges
 448 but no partial factors were computed. The formalism of the *General case* is kept for ease of use
 449 through the adoption of one more favourable buckling curve (in general), similar to the
 450 propositions of Tankova et al. [28] for high strength steel (HSS).

451 A second proposition consists in computing $M_{b,Rd}$ using an alternative expression:

$$M_{b,Rd} = \chi_{LT,mod} \frac{M_{y,Rk}}{\gamma_{M1}} \quad (22)$$

452 where the reduction factor is obtained using Eq. (6) and (7).

453 Expression (22) is inspired from the prescriptions of the *Special case* design method from EN
 454 1993-1-1 [2] (see §6.3.2.3 of the code). This method is not maintained in prEurocode 3 Part 1-1
 455 [1], being replaced with the *new verification format*. Factor f was introduced owing to the
 456 influence of the bending moment distribution on the numerical results (see Figure 6 and Figure
 457 7). The reduction factor χ_{LT} is obtained using expressions (3) and (4) with the following
 458 imperfection factor, adapted to welded beams made of flame-cut flanges:

$$\alpha_{LT} = \frac{0.23}{\lambda_{LT}} \sqrt{\frac{h_t}{b_{\min}}} \quad \text{with } 0.21 \leq \alpha_{LT} \leq 0.49 \quad (23)$$

459 *Proposition II* makes use of an imperfection factor depending on the cross-section depth-to-width
 460 ratio and on the normalized slenderness. Upper and lower limit values of the imperfection factors
 461 are introduced, corresponding to curves *a* and *c*, respectively. The lower bound corresponds to
 462 *Proposition I* imperfection factor and the upper bound to the most favourable buckling curve for
 463 members in bending.

464 An imperfection factor depending on both the slenderness and cross-section dimensions was
 465 introduced due to the distribution of the numerical results. Indeed, the results are closer to *Euler's*
 466 curve as the slenderness increases, which characterizes a diminishing influence of the
 467 imperfections. Making use of the depth-to-width ratio yields a buckling curve per member and is
 468 motivated by the scatter of the numerical results for low and intermediate slenderness. This ratio
 469 is also employed in other existing design methods, such as the French National Annex to Eurocode
 470 3 Part 1-1 [15] that proposes using the following imperfection factor for welded beams:

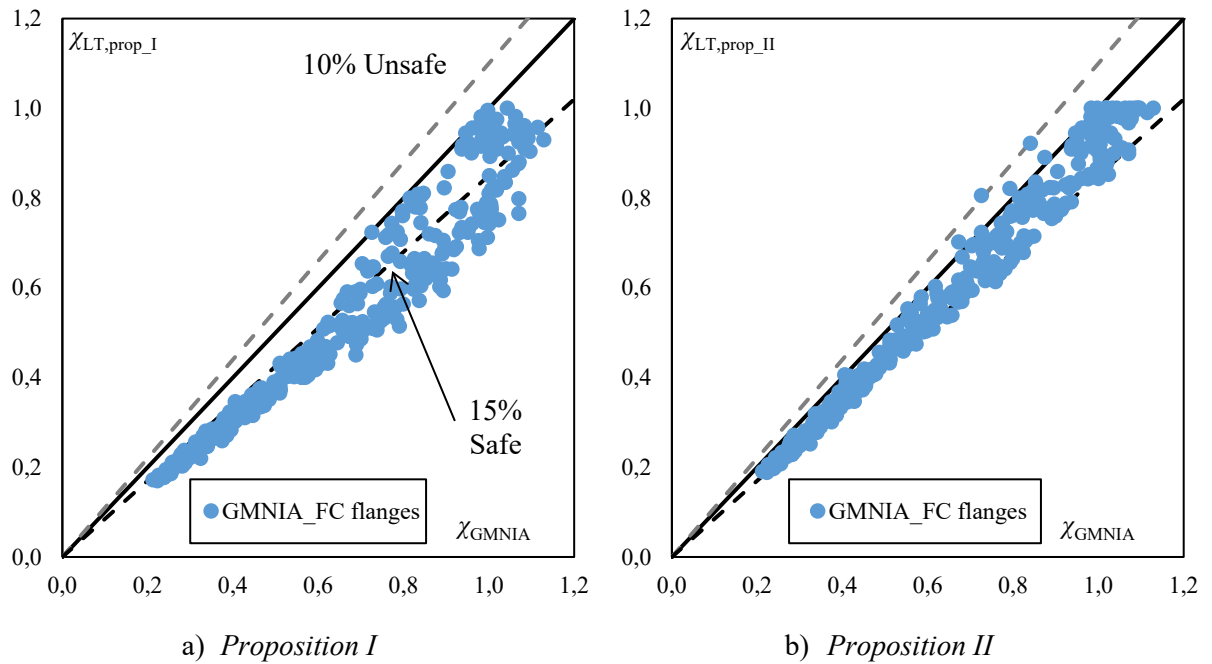
$$\alpha_{LT} = 0.5 - 0.25 \frac{b}{h_t} \lambda_{LT}^{-2} \geq 0 \quad (24)$$

471 Besides, Taras [8] initially introduced imperfection factors depending on the square root of the
 472 depth-to-width ratio. In the final proposal this ratio was replaced with the elastic cross-section
 473 moduli $W_{el,y}/W_{el,z}$, but both ratios are almost proportional.

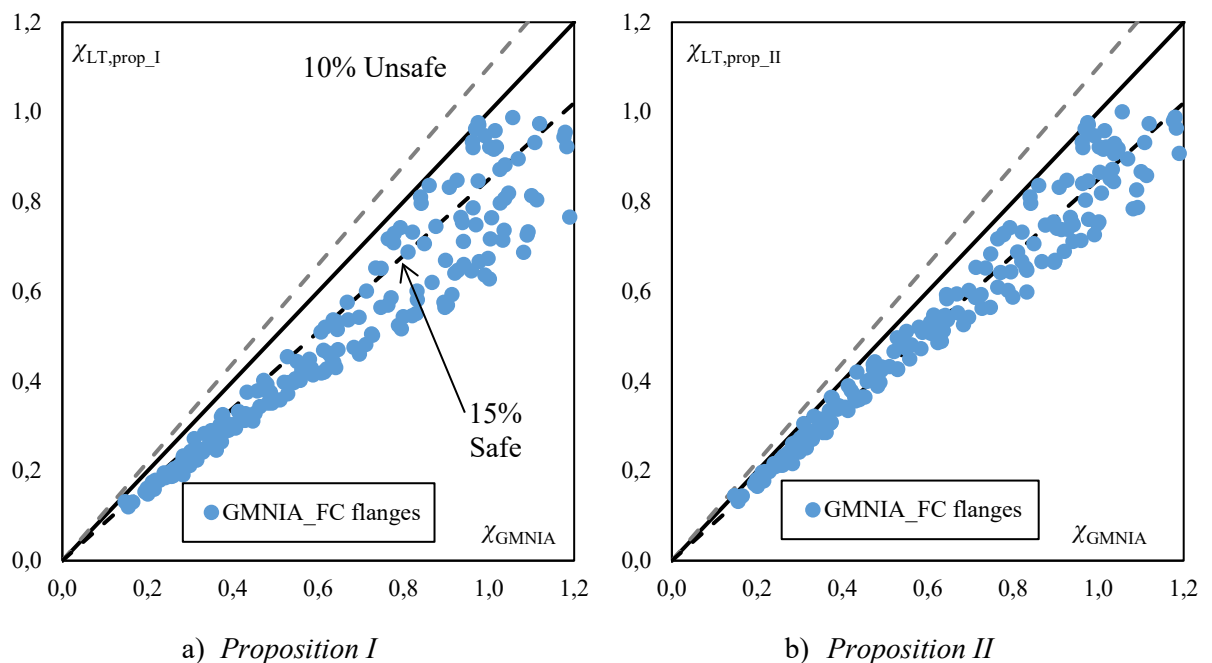
474 The numerical reduction factors are compared against analytical results obtained using
 475 *Propositions I* and *II* in Figure 12 and Figure 13 for beams subjected to end moments with a
 476 doubly or mono-symmetric cross-section, respectively.

477 For doubly symmetric beams, *Proposition I* provides exclusively safe-sided results. The deviation
 478 is small in the low slenderness range, i.e. high reduction factors, ranging from 5% to 10%. The
 479 deviations on the safe side increase for slender members, i.e. between 15% and 25%
 480 approximately. *Proposition II* yields more accurate estimates of the reduction factors. The vast
 481 majority of specimens lie on the safe side with a deviation less than 15%. The few unsafe results

482 correspond to the case of end moments with equal magnitudes but opposite signs inducing shear
 483 in the web. The maximal deviation on the unsafe side is 10%.



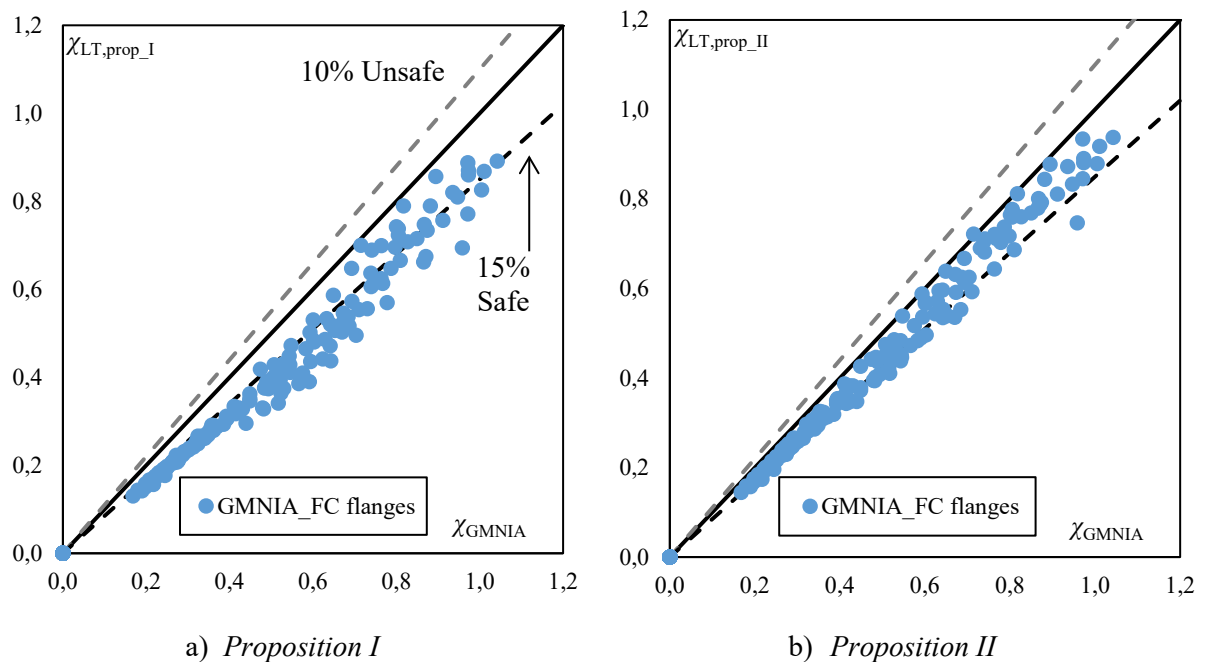
484 **Figure 12: Numerical and analytical reduction factors for uniform doubly symmetric**
 485 **beams under linear bending moment distribution**



486 **Figure 13: Numerical and analytical reduction factors for uniform mono-symmetric**
 487 **beams under linear bending moment distribution**

488 The results are more scattered for mono-symmetric beams, with Figure 13 exhibiting only safe-
 489 sided results for both *Propositions I* and *II*. The scatter is more important for *Proposition I*, which
 490 also provides higher deviations from the numerical results than *Proposition II*.

491 Figure 14 displays the results for doubly and mono-symmetric beams under transverse loading.
 492 All the results lie on the safe side with a mean deviation from the numerical results greater than
 493 25% for *Proposition I* and less than 15% for *Proposition II*. Again, the scatter is more visible for
 494 *Proposition I* than for *Proposition II*.



495 **Figure 14: Numerical and analytical reduction factors for uniform beams under**
 496 **transverse loading**

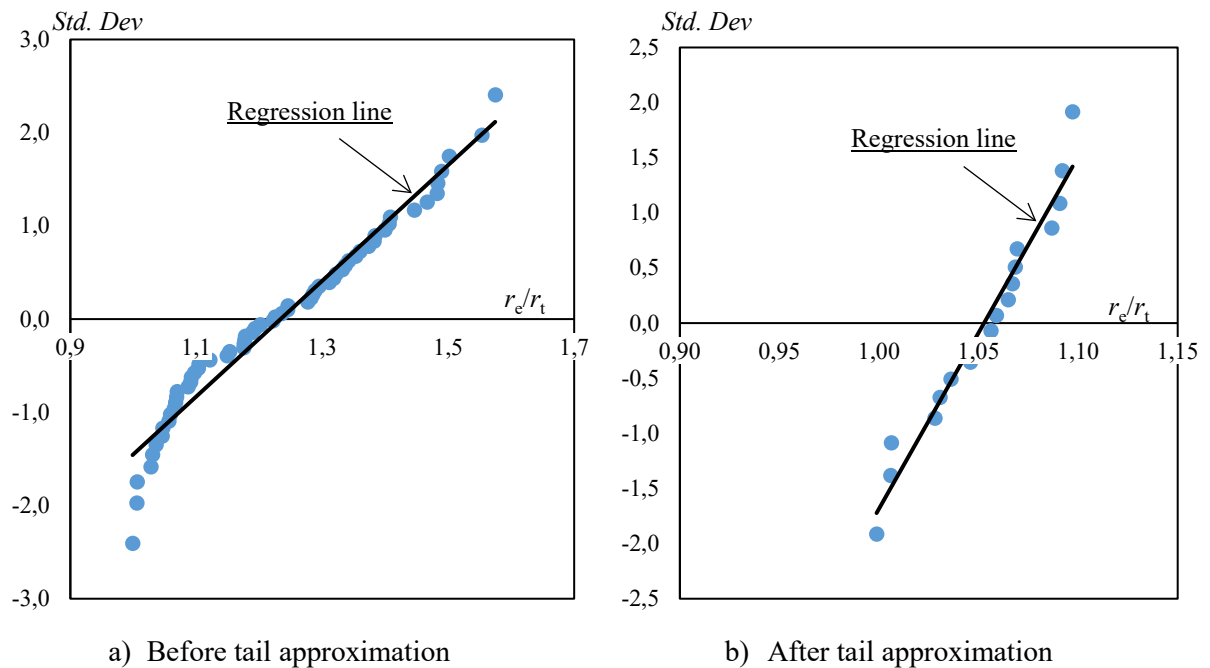
497 The partial factors associated with both *Propositions* are presented in Table 14 for uniform beams
 498 under a linear bending moment distribution with a doubly symmetric or mono-symmetric cross-
 499 section. Table 15 presents the γ_{M1} -values for uniform beams under transverse loading.

500 For doubly symmetric beams, the γ_{M1} values are acceptable for all slenderness ranges of each
 501 method. The partial factors associated with *Proposition II* are closer to unity than those for
 502 *Proposition I* for intermediate and high slenderness. The difference is small in the low slenderness
 503 range.

Design method	Slenderness range	Doubly symmetric		Mono-symmetric	
		n	γ_{M1}	n	γ_{M1}
Proposition I: $\alpha_{LT} = 0.49$	$\bar{\lambda}_{LT} \leq 0.8$	107	0.999	62	<u>1.111</u>
	$0.8 < \bar{\lambda}_{LT} \leq 1.5$	180	0.914	77	0.923
	$1.5 < \bar{\lambda}_{LT}$	100	0.913	57	0.933
	All ranges	387	1.016	196	1.033
Proposition II: $0.21 \leq \alpha_{LT} = \frac{0.23}{\bar{\lambda}_{LT}} \sqrt{\frac{h_t}{b}} \leq 0.49$	$\bar{\lambda}_{LT} \leq 0.8$	107	0.954	62	1.036
	$0.8 < \bar{\lambda}_{LT} \leq 1.5$	180	1.018	77	0.959
	$1.5 < \bar{\lambda}_{LT}$	100	1.021	57	1.031
	All ranges	387	1.025	196	1.014

504 **Table 14: Partial factors of Propositions I and II for uniform beams subjected to end**
 505 **moments**

506 The partial factors associated with Proposition II for mono-symmetric beams are satisfactory for
 507 each slenderness range. The values are close to 1, ranging between 0.96 and 1.04. Using
 508 Proposition I provides more conservative results for medium and high slenderness but appears to
 509 be not acceptable in the low slenderness range. Indeed, a value of 1.11 is obtained owing to
 510 scattered results.



511 **Figure 15: Quantile plot for Proposition I – uniform mono-symmetric beams with low**
 512 **slenderness subjected to end moments**

513 The corresponding quantile plot is presented in Figure 15a), which shows that the results do not
 514 have a normal distribution. A tail approximation is then executed, removing the contributions for
 515 which $r_e/r_t > 1.1$. The resulting quantile plot is presented in Figure 15b). Introducing the tail
 516 approximation reduces the partial factor to 1.02, which is acceptable.

Design method	Slenderness range	n	γ_{M1}
Proposition I: $\alpha_{LT} = 0.49$	$\bar{\lambda}_{LT} \leq 1$	30	0.977
	$1 < \bar{\lambda}_{LT} \leq 1.5$	35	0.930
	$1.5 < \bar{\lambda}_{LT}$	33	0.863
	All ranges	98	0.967
Proposition II: $0.21 \leq \alpha_{LT} = \frac{0.23}{\bar{\lambda}_{LT}} \sqrt{\frac{h_t}{b}} \leq 0.49$	$\bar{\lambda}_{LT} \leq 1$	30	0.976
	$1 < \bar{\lambda}_{LT} \leq 1.5$	35	1.015
	$1.5 < \bar{\lambda}_{LT}$	33	0.971
	All ranges	98	1.006

517 **Table 15: Partial factors of Propositions I and II for uniform beams under transverse**
 518 **loading**

519 The partial factors for beams under transverse loading are also satisfactory for both *Propositions*
 520 for all slenderness ranges. The values for *Proposition I* are low in the intermediate and high
 521 slenderness ranges, being 0.93 and 0.86, respectively, while for *Proposition II* the results are close
 522 to unity in all ranges, i.e. between 0.97 and 1.01. Both *Propositions I* and *II* provide satisfactory
 523 values of partial factors for uniform welded beams made of flame-cut flanges.

524 4.1.1.2 Tapered beams

525 The design value of the lateral-torsional buckling resistance of a tapered welded beam made of
 526 flame-cut flanges can be determined using both proposals (see §4.1.1) with the following specific
 527 adaptations:

- 528 • The h/b ratio accounted for in *Proposition II* and the characteristic resistance $M_{y,Rk}$ are
 529 determined at the cross-section x_α where $\alpha_{ult,k}$ is minimal, which is the critical cross-
 530 section.
- 531 • A term accounting for the tapering of the beam is inserted in the expression of the
 532 imperfection factor of *Proposition II* that becomes:

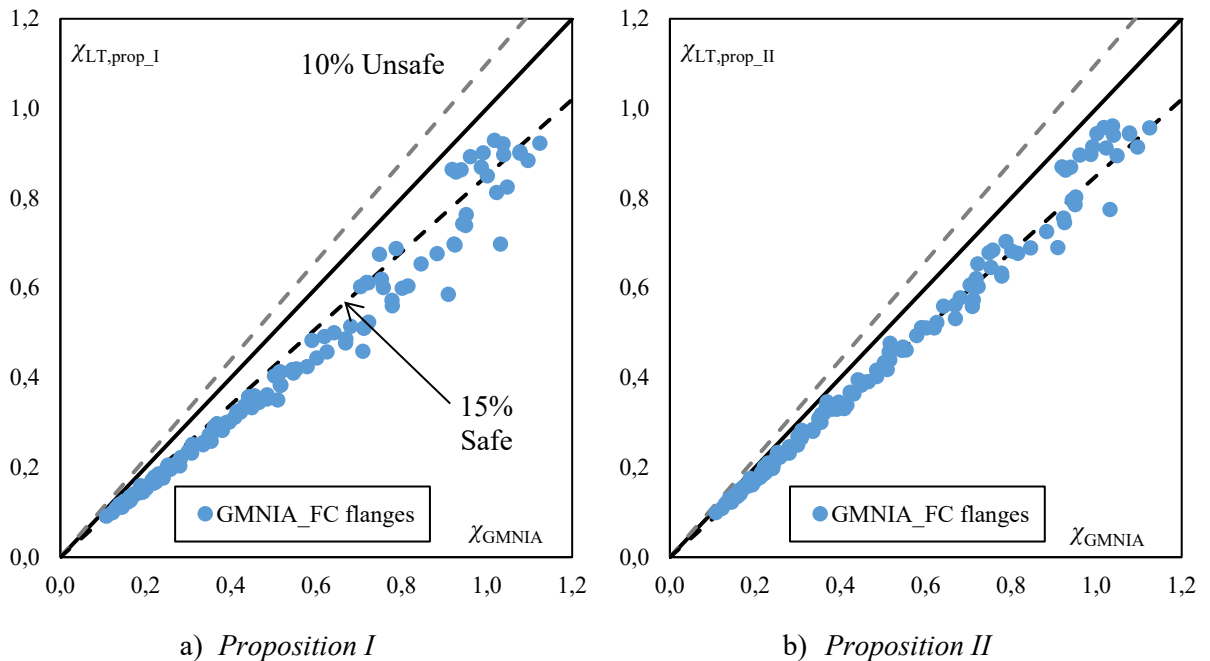
$$\alpha_{LT} = \frac{0.23 + 0.10\gamma}{\bar{\lambda}_{LT}} \sqrt{\frac{h_t}{b_{\min}}} \quad \text{with } 0.21 \leq \alpha_{LT} \leq 0.49 \quad (25)$$

- 533 • The ratio ψ between end moments in the expression of k_c for a linear bending moment
 534 distribution (see Table 3) is replaced with the ratio ψ_ε between bending moment
 535 utilizations at both ends:

$$\psi_\varepsilon = \min \left[\frac{M_{y,Ed}/M_{y,Rk}(x=0)}{\psi M_{y,Ed}/M_{y,Rk}(x=L)}; \frac{\psi M_{y,Ed}/M_{y,Rk}(x=L)}{M_{y,Ed}/M_{y,Rk}(x=0)} \right] \quad (26)$$

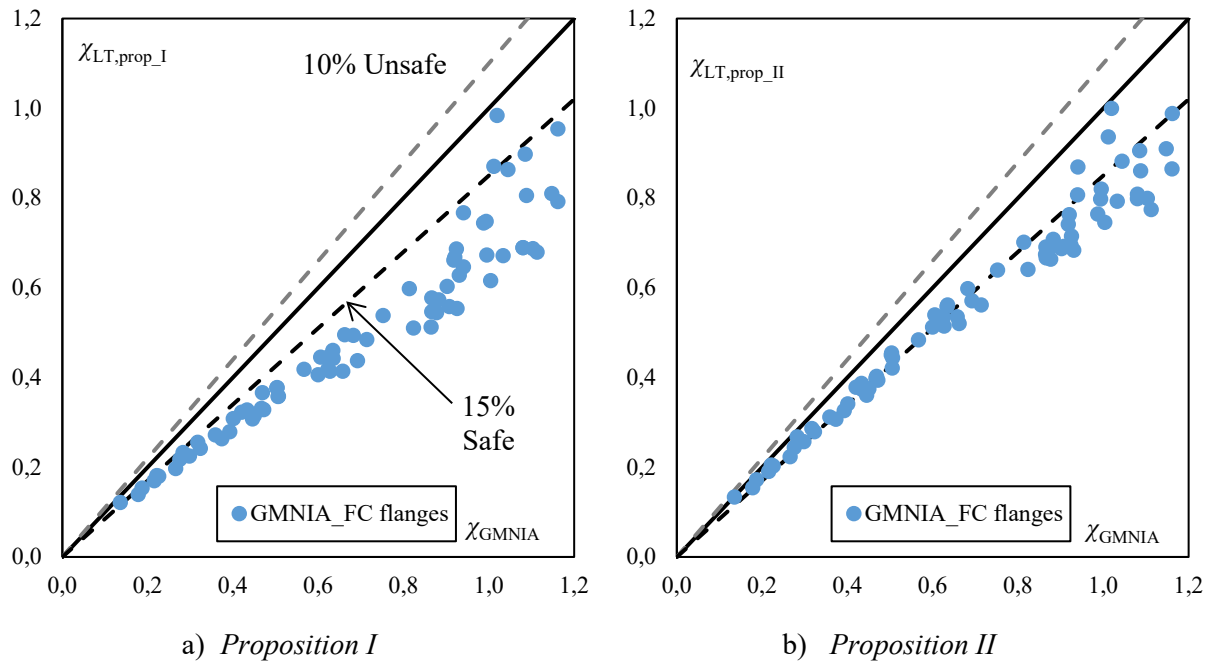
536 A similar approach was used by Marques et al. [10] for the adaptation of the interaction
 537 formulae to tapered members. The C_{mi} coefficients were indeed expressed as a function
 538 of ψ_ε instead of ψ .

539 The numerical and analytical reduction factors of tapered doubly symmetric beams are compared
 540 in Figure 16 for both *Propositions*. Figure 17 presents the results for tapered mono-symmetric
 541 beams.



542 **Figure 16: Numerical and analytical reduction factors for tapered doubly symmetric**
 543 **beams**

544 In the case of doubly symmetric beams, all results are on the safe side for both proposals.
 545 *Proposition I* provides more scattered results than *Proposition II* and a larger average deviation
 546 from the reference numerical results. While the average deviation is greater than 15% for
 547 *Proposition I*, it ranges between 5% and 10% for *Proposition II*.



548 **Figure 17: Numerical and analytical reduction factors for tapered mono-symmetric beams**

549 All of the results also lie on the safe side for mono-symmetric beams. Results obtained with
 550 *Proposition II* are scattered in the low slenderness range. The scatter is more pronounced for
 551 *Proposition I*, in particular for low and intermediate slenderness. For both types of cross-sections,
 552 *Proposition II* produces more accurate predictions of the lateral-torsional buckling resistance than
 553 *Proposition I*.

554 The partial factors associated with both *Propositions I* and *II* are presented in Table 16 for doubly
 555 and mono-symmetric beams. The values for doubly symmetric beams are very close to unity for
 556 *Proposition II*. Lower values, between 0.92 and 1, are obtained for *Proposition I*. The partial
 557 factors for tapered mono-symmetric beams are lower than those for doubly symmetric beams.
 558 The values range between 0.93 and 0.99 for *Proposition II* while greater deviations from unity
 559 are observed for *Proposition I*. Indeed, in the medium slenderness range, a partial factor of 0.85
 560 is encountered, corresponding to a somewhat conservative design method.

Design method	Doubly symmetric			Mono-symmetric		
	Slenderness range	n	γ_{M1}	Slenderness range	n	γ_{M1}
Proposition I: $\alpha_{LT} = 0.49$	$\bar{\lambda}_{LT} \leq 0.8$	26	1.003	$\bar{\lambda}_{LT} \leq 0.8$	38	0.940
	$0.8 < \bar{\lambda}_{LT} \leq 1.5$	42	0.921	$0.8 < \bar{\lambda}_{LT} \leq 1.25$	28	0.848
	$1.5 < \bar{\lambda}_{LT}$	61	0.945	$1.25 < \bar{\lambda}_{LT}$	29	0.925
	All ranges	129	0.975	All ranges	95	0.911
Proposition II: $0.21 \leq \alpha_{LT} = \frac{0.23 + 0.10\gamma}{\bar{\lambda}_{LT}} \sqrt{\frac{h_t}{b}} \leq 0.49$	$\bar{\lambda}_{LT} \leq 0.8$	26	1.003	$\bar{\lambda}_{LT} \leq 0.8$	38	0.970
	$0.8 < \bar{\lambda}_{LT} \leq 1.5$	42	0.958	$0.8 < \bar{\lambda}_{LT} \leq 1.25$	28	0.929
	$1.5 < \bar{\lambda}_{LT}$	61	1.038	$1.25 < \bar{\lambda}_{LT}$	29	0.993
	All ranges	129	1.015	All ranges	95	0.972

561 **Table 16: Partial factors of both *Propositions* for tapered beams**

562 Similar to the case of uniform beams, the two proposals are characterized by appropriate values
 563 of partial factors for tapered welded beams made of flame-cut flanges. For both types of beams
 564 and both types of cross-sections, *Proposition II* produces more accurate estimates of the buckling
 565 resistance than *Proposition I*.

566 **4.1.2 Welded beams made of hot-rolled flanges**

567 A single proposal is made for uniform doubly symmetric welded beams with hot-rolled flanges
 568 that consists in computing $M_{b,Rd}$ using expression (22) i.e. making use of the factor f . The
 569 reduction factor χ_{LT} is computed with expressions (3) and (4) with the following imperfection
 570 factor:

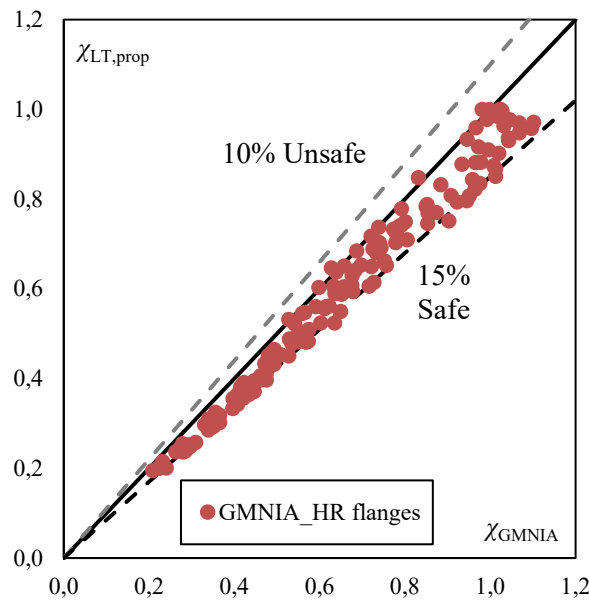
$$\alpha_{LT} = \frac{0.30}{\bar{\lambda}_{LT}} \sqrt{\frac{h_t}{b}} \quad \text{with } 0.21 \leq \alpha_{LT} \leq 0.76 \quad (27)$$

571 This proposal is very close to *Proposition II* presented for welded beams with flame-cut flanges.
 572 Similar to the case of welded beams with flame-cut flanges, the previous imperfection factor (27)
 573 was used because of the discrepancy of the numerical results. Differences between expressions
 574 (23) and (27) regard:

- 575 • The multiplying coefficient of the imperfection factor that is 0.23 for flame-cut flanges
 576 and 0.30 for hot-rolled flanges, and

- 577 • The lower bound of α_{LT} that corresponds to buckling curve c and d for flame-cut and hot-
 578 rolled flanges, respectively.

579 The numerical and analytical reduction factors are compared in Figure 18. The vast majority of
 580 the analytical results are on the safe side with a deviation from the numerical results of less than
 581 15%. The proposal for uniform doubly symmetric welded beams made of hot-rolled flanges
 582 provides accurate estimates of the numerical results.



583

584 **Figure 18: Numerical and analytical reduction factors for uniform doubly symmetric**
 585 **beams**

586 The partial factors associated with this proposal for uniform doubly symmetric welded beams
 587 made of hot-rolled flanges are given in Table 17. The values are close to unity for the three
 588 slenderness ranges with a maximal value of 1.03. The proposal is associated with appropriate
 589 values of partial factors for uniform doubly symmetric welded beams made of hot-rolled flanges.

Slenderness range	n	γ_{M1}
$\bar{\lambda}_{LT} \leq 0.8$	52	0.951
$0.8 < \bar{\lambda}_{LT} \leq 1.5$	72	0.997
$1.5 < \bar{\lambda}_{LT}$	30	1.032
All ranges	154	0.997

590

Table 17: Partial factors of the proposal for beams with hot-rolled flanges

4.2 Adaptation of the new verification format

4.2.1 Analytical developments

The consistent derivation of the *new verification format* of prEurocode 3 Part 1-1 [1] was presented by Taras (see [8], [9]) for uniform doubly symmetric beams. However, an extension of the scope of this method is certainly needed and particularly for tapered and/or mono-symmetric beams, which are commonly used in practice. A tapered mono-symmetric beam subjected to a constant bending moment distribution is first investigated, as depicted in Figure 19. The linear bending moment distribution is considered next.

The design method is based on the expression of the first yield criterion:

$$\frac{M_{y,Ed}}{M_{y,Rk}}(x) + \frac{M_{z,Ed}^{\text{II}}}{M_{z,Rk}}(x) + \frac{B_{Ed}^{\text{II}}}{B_{Rk}}(x) = 1.0 \quad (28)$$

with:

$M_{z,Ed}^{\text{II}}$: maximum design value of the second order bending moment about z - z ,

$M_{z,Rk}$: characteristic value of the cross-section resistance against bending about z - z ,

B_{Ed}^{II} : maximum design value of the second order bimoment,

B_{Rk} : characteristic value of the cross-section resistance to bimoment.

The distributions of the internal stresses of the flanges owing to the first order in-plane bending moment M_y , second order out-of-plane bending moment M_z and bimoment B are presented in Figure 20. For mono-symmetric beams, the first yield may be encountered at the most compressed end of the compressive flange (case depicted in Figure 20). Failure can alternatively be due to the superposition of tensile stresses owing to M_z and B in the tensile flange.

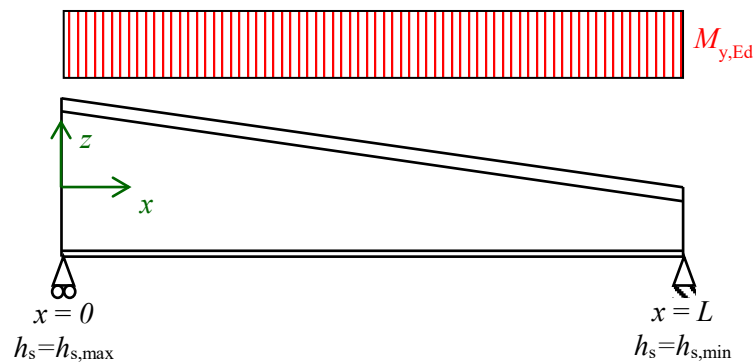


Figure 19: Configuration for extending the scope of the *new verification format*

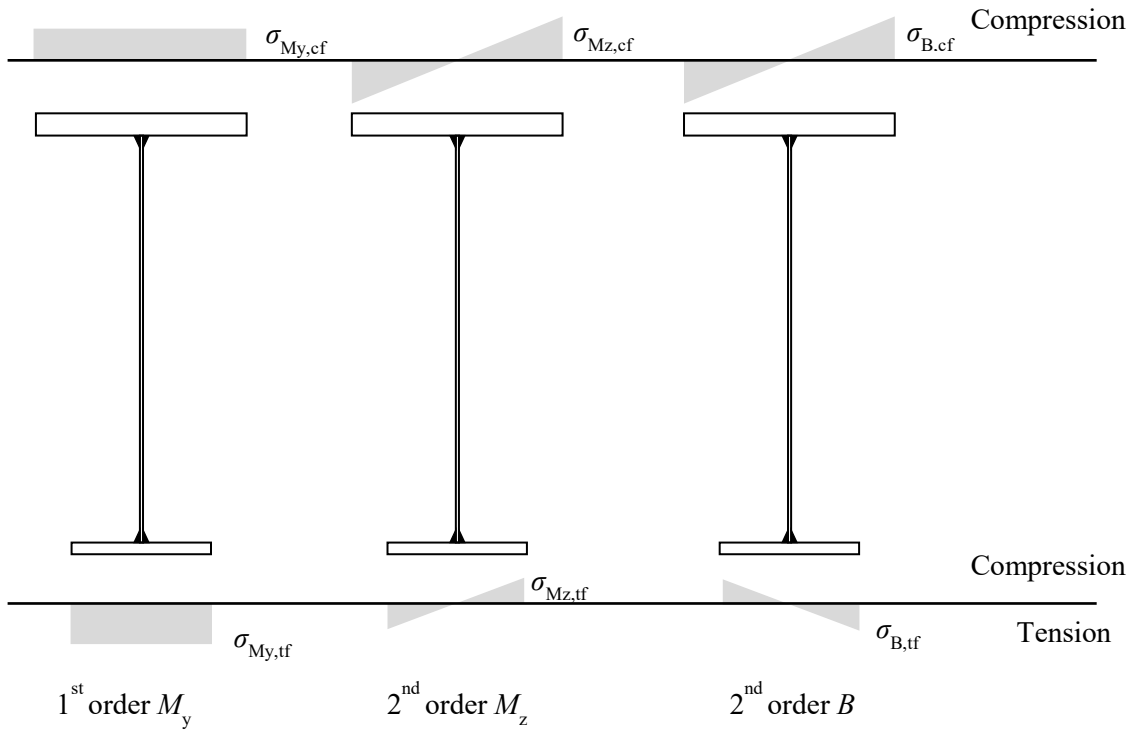
612 To deal with these two possible failure modes, the verification format of expression (28) is
 613 simplified as follows:

$$\frac{M_{y,Ed}(x)}{M_{y,Rk}} + \max \varepsilon_{Mz}(x) + \max \varepsilon_B(x) = 1.0 \quad (29)$$

614 with:

$$\varepsilon_{Mz}(x) = \frac{M_{z,Ed}^{\text{II}}(x)}{M_{z,Rk}} \quad (30)$$

$$\varepsilon_B(x) = \frac{B_{Ed}^{\text{II}}(x)}{B_{Rk}} \quad (31)$$



615

616

Figure 20: Stresses in beam flanges

617 The elastic cross-sectional resistances against out-of-plane bending moment M_z and bimoment B
 618 are:

$$M_{z,Rk} = W_z f_y \quad (32)$$

$$B_{Rk}(x) = \frac{I_w(x)}{\omega_{\max}(x)} f_y \quad (33)$$

619 where in the general case of a mono-symmetric beam:

$$W_z = \frac{I_z}{\max(b_t; b_c)/2} \quad (34)$$

$$\omega_{\max}(x) = \frac{\max(b_t z_{ft}(x); b_c z_{fc}(x))}{2} \quad (35)$$

620 where z_{ft} and z_{fc} are the distance between the cross-section shear centre and the centroid of the
 621 tensile and compressive flanges, respectively (see Figure 21) and are obtained using:

$$z_{ft}(x) = \frac{I_{z,fc}}{I_z} h(x) \quad (36)$$

$$z_{fc}(x) = \frac{I_{z,ft}}{I_z} h(x) \quad (37)$$

622 Besides, the distance between both flanges centroids at each location, $h(x)$, varies linearly
 623 according to:

$$h(x) = h_{s,\max} \bar{h}(x) \quad (38)$$

624 with:

625 $h_{s,\max}$ is the distance between the flange centroids at the highest cross-section (see Figure 19).

$$626 \quad \bar{h}(x) = 1 - \gamma \frac{x}{L}$$

$$627 \quad \gamma = 1 - \frac{h_{s,\min}}{h_{s,\max}}$$

628 The effects of both bending moments and the bimoment are all treated separately using the safe-
 629 sided assumption that failure occurs when they all reach their maximal values.

630 To determine the acting second order out-of-plane bending moment and bimoment, it is assumed
 631 that:

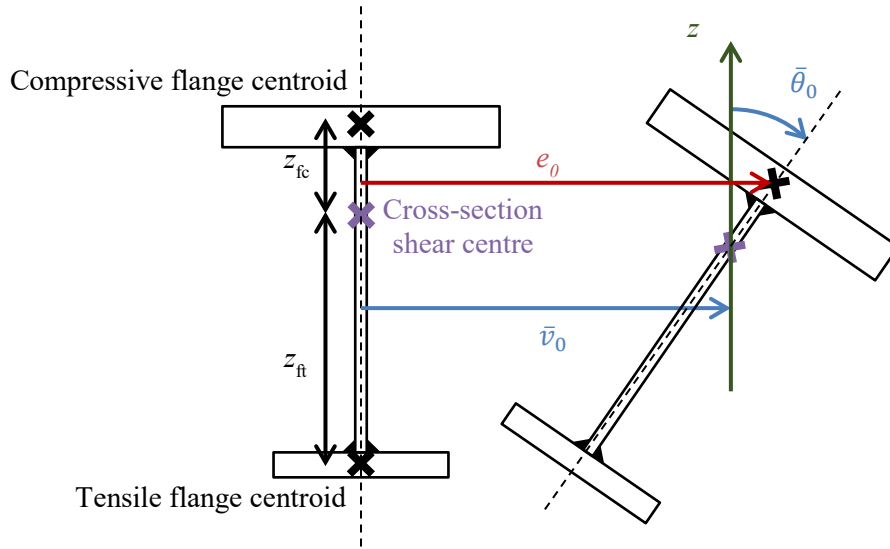
$$\frac{\bar{v}_{cr}}{\bar{\theta}_{cr}} = \frac{\bar{v}_0}{\bar{\theta}_0} = \frac{M_{y,cr}}{N_{cr,z}} \quad (39)$$

632 where the indexes “cr” and “0” refer to the elastic critical mode shape and to the initial
 633 imperfections, respectively. Besides, $N_{cr,z}$ is the elastic critical out-of-plane flexural buckling load.

634 The use of expression (39) implies that the initial imperfections are analogous to the critical mode
 635 shapes with different amplitudes. The shape functions for the twist rotation and lateral
 636 displacement are indeed assumed homothetic to half a sine wave:

$$v(x) = \bar{v}_0 \sin\left(\frac{\pi x}{L}\right) \quad (40)$$

$$\theta(x) = \bar{\theta}_0 \sin\left(\frac{\pi x}{L}\right) \quad (41)$$



637

638

Figure 21: Initial imperfections

639 The following amplification relationships are used:

$$v(x) = \frac{1}{\alpha_{cr} - 1} v_0(x) \quad (42)$$

$$\theta(x) = \frac{1}{\alpha_{cr} - 1} \theta_0(x) \quad (43)$$

640 with:

$$\alpha_{cr} = \frac{M_{y,cr}}{M_{y,Ed}} \quad (44)$$

641 In addition, the second order out-of-plane bending moment M_z and bimoment B are:

$$M_{z,Ed}^{\text{II}}(x) = -EI_z \frac{d^2 v}{dx^2}(x) \quad (45)$$

$$B_{\text{Ed}}^{\text{II}}(x) = -EI_w(x) \left(\frac{d^2\theta}{dx^2}(x) + \frac{2}{h(x)} \frac{d\theta}{dx}(x) \frac{dh}{dx}(x) \right) \quad (46)$$

642 where the bimoment expression accounts for the flanges inclination, as derived by Kitipornchai
643 et al. ([25], [26]) for doubly and mono-symmetric tapered beams.

644 Inserting expressions (39) – (43) and (38) into (45) and (46) yields:

$$M_{z,\text{Ed}}^{\text{II}}(x) = EI_z \frac{M_{y,\text{cr}}}{N_{\text{cr},z}} \frac{1}{\frac{M_{y,\text{cr}}}{M_{y,\text{Ed}}} - 1} \bar{\theta}_0 \left(\frac{\pi}{L} \right)^2 \sin\left(\frac{x\pi}{L} \right) \quad (47)$$

$$B_{\text{Ed}}^{\text{II}}(x) = \frac{EI_z}{M_{y,\text{cr}}} \left(\frac{\pi}{L} \right)^2 \frac{I_w(x)}{I_z} \frac{M_{y,\text{Ed}}}{1 - \frac{M_{y,\text{Ed}}}{M_{y,\text{cr}}}} \bar{\theta}_0 \left(\sin\left(\frac{x\pi}{L} \right) + \frac{2\gamma}{\pi h(x)} \cos\left(\frac{x\pi}{L} \right) \right) \quad (48)$$

645 Using expressions (32) – (35) along with (47) and (48), the maximal values of the utilization ratios
646 ε_{Mz} for the out-of-plane bending moment and ε_{B} for the bimoment are:

$$\max \varepsilon_{\text{Mz}}(x) = \frac{1}{W_{zfy}} \frac{M_{y,\text{Ed}}}{1 - \frac{M_{y,\text{Ed}}}{M_{y,\text{cr}}}} \bar{\theta}_0 \quad (49)$$

$$\max \varepsilon_{\text{B}}(x) = \varepsilon_{\text{B}}(x_0) = \frac{N_{\text{cr},z}}{M_{y,\text{cr}}} \frac{\bar{\omega}}{W_{zfy}} \frac{M_{y,\text{Ed}}}{1 - \frac{M_{y,\text{Ed}}}{M_{y,\text{cr}}}} \bar{\theta}_0 g(x_0) \quad (50)$$

647 with:

$$\bar{\omega} = \frac{h_{s,\text{max}}}{I_z} \frac{\max(b_t I_{z,\text{fc}}; b_c I_{z,\text{ft}})}{\max(b_t; b_c)} \quad (51)$$

648 and:

$$g(x_0) = \bar{h}(x_0) \sin\left(\frac{x_0\pi}{L} \right) + \frac{2\gamma}{\pi} \cos\left(\frac{x_0\pi}{L} \right) \quad (52)$$

649 The bimoment utilization ratio reaches its peak value at the location x_0 obtained when:

$$\frac{\partial g}{\partial x}(x_0) = 0 \quad (53)$$

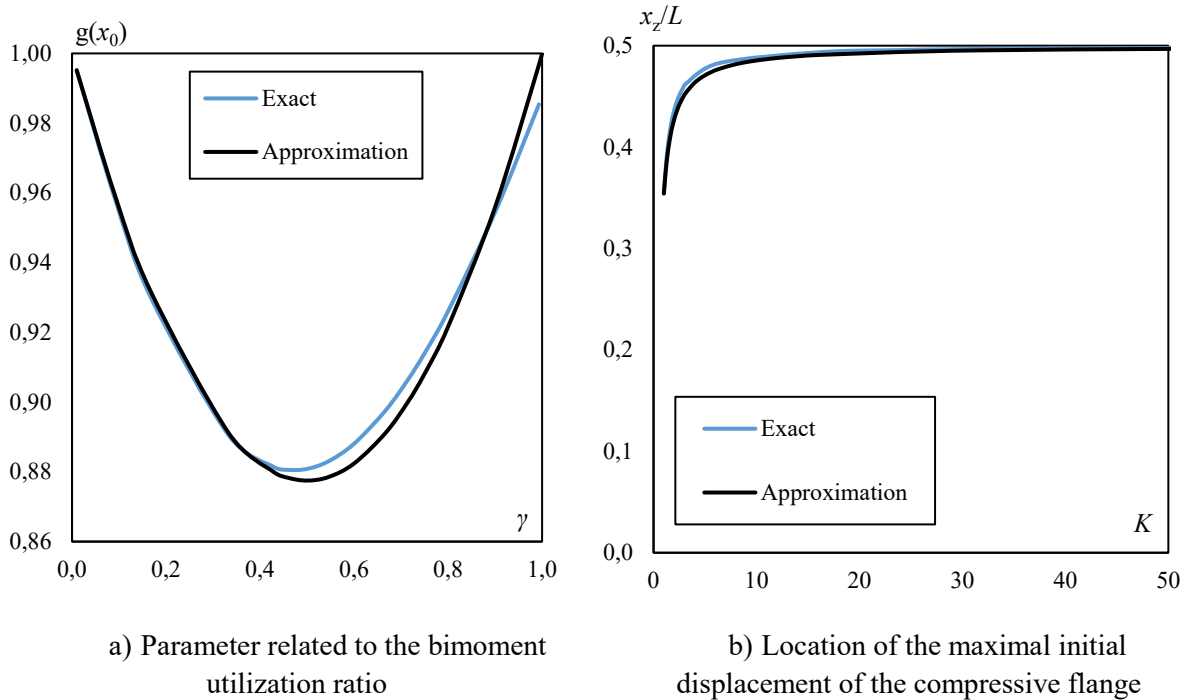
650 i.e.:

$$\bar{h}(x_0) \cos\left(\frac{x_0\pi}{L}\right) - \frac{3\gamma}{\pi} \sin\left(\frac{x_0\pi}{L}\right) = 0 \quad (54)$$

651 The exact values of x_0/L are determined using the previous expression and the corresponding
 652 values of $g(x_0)$ are obtained using Eq. (52). The results are presented in Figure 22a) as a function
 653 of γ . The predictions of the following approximate expression are also presented:

$$f(\gamma) = 0.49\gamma(\gamma - 1) + 1 \quad (55)$$

654 The maximum difference between exact and approximated values is less than 2%.



655 **Figure 22: Approximations employed for the design method**

656 Expression (29) is consequently rewritten as:

$$\frac{M_{y,Ed}}{M_{y,Rk}(x)} + \frac{1}{W_z f_y} \frac{M_{y,Ed}}{1 - \frac{M_{y,Ed}}{M_{y,cr}}} \bar{\theta}_0 \left[1 + \frac{N_{cr,z}}{M_{y,cr}} \bar{\omega} f(\gamma) \right] = 1.0 \quad (56)$$

657 The remaining unknown corresponding to the initial torsional twist amplitude can be expressed
 658 as a function of the imperfection amplitude e_0 measured in the compressive flange (see Figure
 659 21), as assumed by Taras ([8], [9]):

$$e_0 = \bar{v}_0 + z_{fc}(x_z)\bar{\theta}_0 = \left(\frac{M_{y,cr}}{N_{cr,z}} + z_{fc}(x_z) \right) \bar{\theta}_0 \quad (57)$$

660 where x_z is the location of the cross-section where the initial out-of-plane displacement of the
 661 compressive flange reaches its maximal value.

662 It should be noted that the following simplifying assumption is introduced in the right-hand side
 663 of expression (57):

$$\sin\left(\frac{x_z\pi}{L}\right) \approx 1 \quad (58)$$

664 This simplification makes use of the peak value of the sine function and therefore increases the
 665 right-hand side of equation (57), providing greater values of e_0 than the “actual” e_0 values.
 666 Introducing this simplification in (57) can then not provide underestimated values of e_0 i.e. unsafe
 667 results. Besides, expression (58) is appropriate when x_z is close to mid-span, otherwise results
 668 obtained using equation (57) might be overly conservative.

669 To determine the value of x_z , one may express the initial displacement of the compressive flange
 670 δ_{fl} along the beam:

$$\delta_{fl}(x) = \left(\frac{M_{y,cr}}{N_{cr,z}} + z_{fc}(x) \right) \sin\left(\frac{x\pi}{L}\right) \bar{\theta}_0 \quad (59)$$

671 One obtains x_z when:

$$\frac{\partial \delta_{fl}}{\partial x}(x_z) = 0 \quad (60)$$

672 i.e.:

$$\pi K = \frac{x_z\pi}{L} + \tan\left(\frac{x_z\pi}{L}\right) \quad (61)$$

673 with:

$$674 \quad K = \frac{1}{\gamma} \left[\frac{M_{y,cr} I_z}{N_{cr,z} I_{z,ft} h_{s,max}} + 1 \right]$$

675 The actual value of x_z is plotted with respect to the parameter K in Figure 22b). The predictions
 676 of the following approximation are added for comparison:

$$\frac{x_z}{L} = 0.5 - \frac{0.146}{K} \quad (62)$$

677 Very close results are obtained using expressions (60) and (62), and x_z barely diverges from mid-
678 span in most cases. This is in line with the previous approximation of Eq. (58).

679 Inserting expression (62) into (38) results in:

$$\bar{h}(x_z) = 1 - 0.5\gamma + \frac{0.146\gamma}{K} \quad (63)$$

680 Finally, expression (56) is rewritten as:

$$\frac{M_{y,Ed}}{M_{y,Rk}(x)} + \frac{1}{W_z f_y} \frac{M_{y,Ed}}{1 - \frac{M_{y,Ed}}{M_{y,cr}}} e_0 \frac{1 + \frac{N_{cr,z}}{M_{y,cr}} \bar{\omega} f(\gamma)}{\frac{M_{y,cr}}{N_{cr,z}} + h_{s,max} \frac{I_{z,ft}}{I_z} \bar{h}(x_z)} = 1.0 \quad (64)$$

681 which can be expressed as:

$$\frac{M_{y,Ed}}{M_{y,Rk}(x)} \left\{ 1 + \frac{e_0}{1 - \frac{M_{y,Ed}}{M_{y,cr}}} \frac{A(x) W_y(x) f_y N_{cr,z}}{W_z A(x) f_y M_{y,cr}} \xi \right\} = 1.0 \quad (65)$$

682 where the parameter ξ accounts for the tapering and mono-symmetric design of the member and
683 is given by:

$$\xi = \frac{\frac{M_{y,cr}}{N_{cr,z}} + \bar{\omega} f(\gamma)}{\frac{M_{y,cr}}{N_{cr,z}} + h_{s,max} \frac{I_{z,ft}}{I_z} \bar{h}(x_z)} \quad (66)$$

684 In the particular case of a doubly symmetric beam, ξ is reduced to:

$$\xi = \frac{\frac{M_{y,cr}}{N_{cr,z}} + \frac{h_{s,max}}{2} f(\gamma)}{\frac{M_{y,cr}}{N_{cr,z}} + \frac{h_{s,max}}{2} \bar{h}(x_z)} \quad (67)$$

685 In the more specific case of a uniform and doubly symmetric beam, ξ is reduced to unity and
686 expression (65) can be found in the derivation of the *new verification format* by Taras ([8], [9]).

687 The following dimensionless parameters are introduced:

$$\bar{\lambda}_{LT}(x) = \sqrt{\frac{M_{y,Rk}(x)}{M_{y,cr}}} \quad (68)$$

$$\bar{\lambda}_z(x) = \sqrt{\frac{N_{Rk}(x)}{N_{cr,z}}} \quad (69)$$

$$\chi_{LT}(x) = \frac{M_{y,Ed}}{M_{y,Rk}(x)} \quad (70)$$

688 and inserted into expression (65), yielding:

$$\chi_{LT}(x) + \frac{\chi_{LT}(x)}{1 - \chi_{LT}(x)\bar{\lambda}_{LT}^2} \left(\frac{\bar{\lambda}_{LT}(x)}{\bar{\lambda}_z(x)} \right)^2 \eta(x)\xi = 1.0 \quad (71)$$

689 where the generalized imperfection η stands for:

$$\eta(x) = e_0 \frac{A(x)}{W_z} \quad (72)$$

690 Expression (71) is similar to that obtained by Taras ([8], [9]) in the particular case of a uniform
 691 doubly symmetric beam, ξ being equal to unity in such case. A vast parametric study was
 692 conducted leading to the following proposition for the generalized imperfection:

$$\eta = \alpha_{LT} (\bar{\lambda}_z - 0.2) \quad (73)$$

693 where the imperfection factor α_{LT} is given in Table 4 for welded beams. A coefficient f_M was also
 694 introduced to account for the bending moment distribution (see Table 3).

695 For the sake of simplicity, it is proposed to retain expression (73) for the generalized imperfection
 696 in the case of tapered mono-symmetric beams. The following expression of f_M , adapted to non-
 697 uniform beams, is proposed in the case of a linear bending moment distribution:

$$f_{M,\varepsilon} = 1.25 - 0.1\psi_\varepsilon - 0.15\psi_\varepsilon^2 \quad (74)$$

698 where the ratio ψ_ε between the end moment utilizations is given by:

$$\psi_\varepsilon = \min \left[\frac{M_{y,Ed}/M_{y,Rk}(x=0)}{\psi M_{y,Ed}/M_{y,Rk}(x=L)}; \frac{\psi M_{y,Ed}/M_{y,Rk}(x=L)}{M_{y,Ed}/M_{y,Rk}(x=0)} \right] \quad (75)$$

699 The beam stability must be verified at the cross-section x_α .

700 An adaptation of the *new verification format* from prEurocode 3 Part 1-1 [1] was derived to extend
 701 its scope to tapered mono-symmetric beams. For such members, the design method requires that
 702 the following be verified:

$$\frac{M_{y,Ed}(x_\alpha)}{M_{b,Rd}(x_\alpha)} \leq 1.0 \quad (76)$$

703 with:

$$M_{b,Rd}(x_\alpha) = \chi_{LT}(x_\alpha) \frac{M_{y,Rk}(x_\alpha)}{\gamma_{M1}} \quad (77)$$

$$\chi_{LT}(x_\alpha) = \frac{f_{M,\varepsilon}}{\phi_{LT}(x_\alpha) + \sqrt{\phi_{LT}^2(x_\alpha) - f_{M,\varepsilon} \bar{\lambda}_{LT}^2(x_\alpha)}} \leq 1.0 \quad (78)$$

$$\phi_{LT}(x_\alpha) = 0.5 \left[1 + f_{M,\varepsilon} \left(\left(\frac{\bar{\lambda}_{LT}(x_\alpha)}{\bar{\lambda}_z(x_\alpha)} \right)^2 \alpha_{LT}(x_\alpha) (\bar{\lambda}_z(x_\alpha) - 0.2) \xi + \bar{\lambda}_{LT}^2(x_\alpha) \right) \right] \quad (79)$$

704 The imperfection factors α_{LT} for welded beams are given in Table 4 in the case of uniform beams.
 705 For tapered members, the same expressions could be used where both cross-section elastic moduli
 706 are computed at $x = x_\alpha$.

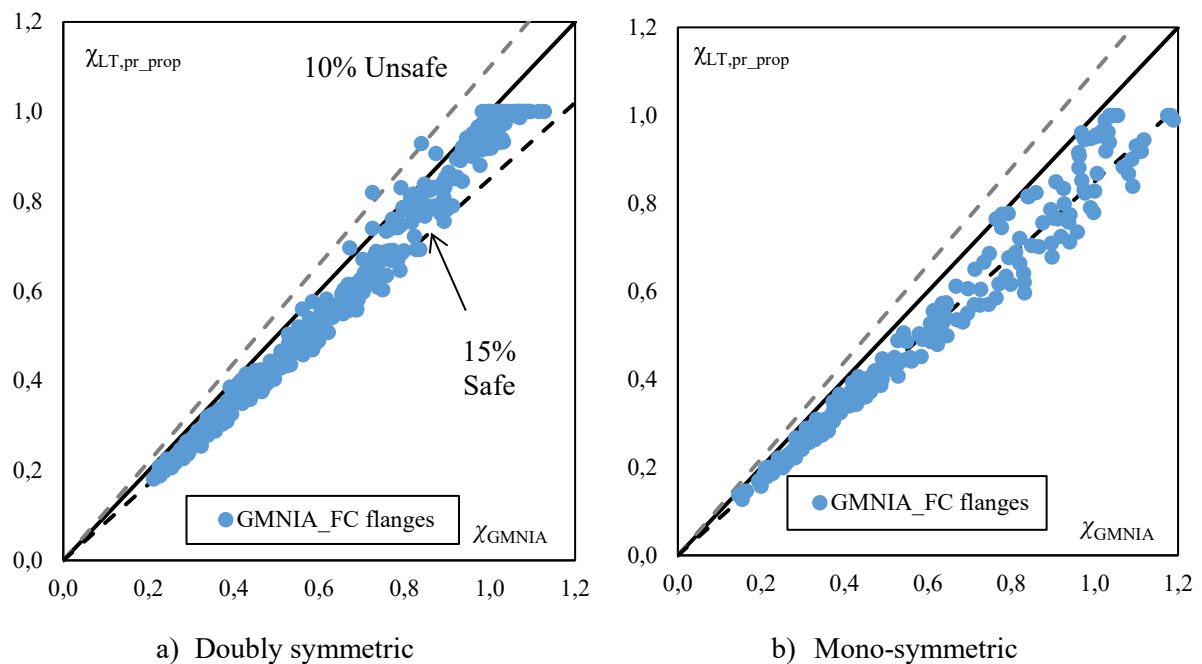
707 4.2.2 Propositions for welded beams made of flame-cut flanges

708 The design value of the lateral-torsional buckling resistance of tapered mono-symmetric beams
 709 can be obtained using expressions (77) – (79). The following imperfection factor is proposed for
 710 welded beams made of flame-cut flanges with $t_f \leq 40$ mm:

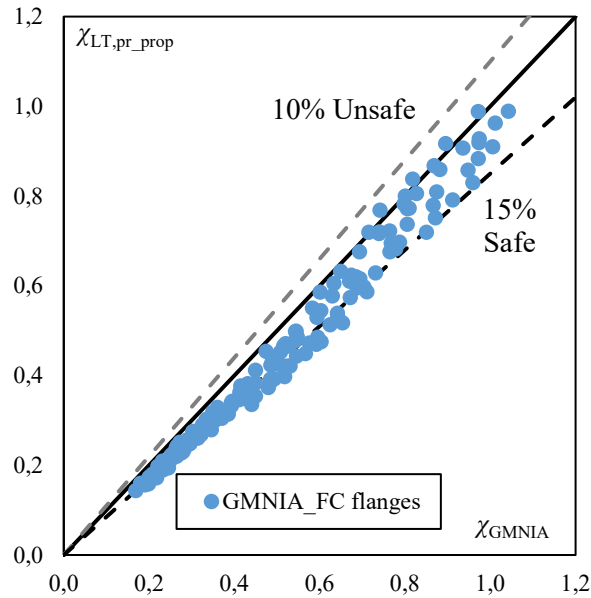
$$\alpha_{LT}(x_\alpha) = 0.21 \sqrt{\frac{W_{el,y}(x_\alpha)}{W_{el,z}}} \leq 0.49 + 0.15\gamma \quad (80)$$

711 To keep the formalism of the imperfection factors from prEurocode 3 [1], a simple adaptation is
 712 introduced in this *Proposition III*. Indeed, Eq. (80) is similar to that of Table 4 for $t_f \leq 40$ mm
 713 except for the upper limit. A value of 0.64 is currently prescribed but a smaller value is proposed,
 714 ranging between 0.49 and 0.64 depending on the tapering of the member. For uniform beams, the
 715 boundary is set to 0.49. The results of *Proposition III* are tested against the numerical results in
 716 Figure 23 and Figure 24 for uniform beams subjected to a linear bending moment distribution or

717 a transverse loading, respectively. Figure 25 displays the results for tapered beams. For uniform
 718 beams, the analytical results are close to the numerical ones and a low scatter is observed. A few
 719 results are non-conservative for doubly symmetric beams under end moments when $\psi = -1$. The
 720 predictions for mono-symmetric beams are all safe-sided.
 721 Most results obtained for beams under transverse loading are on the safe side with a deviation
 722 from the numerical results of less than 15%. The maximal deviation on the unsafe side is 4% and
 723 corresponds to cases with significant shear, i.e. the cross-section resistance to bending should be
 724 reduced owing to shear effects, according to both versions of Eurocode 3 Part-1-1 ([1], [2]). All
 725 results lie on the safe side for tapered doubly symmetric beams also with a low scatter. The scatter
 726 is slightly more significant in the case of tapered mono-symmetric beams where more
 727 conservative results are obtained.



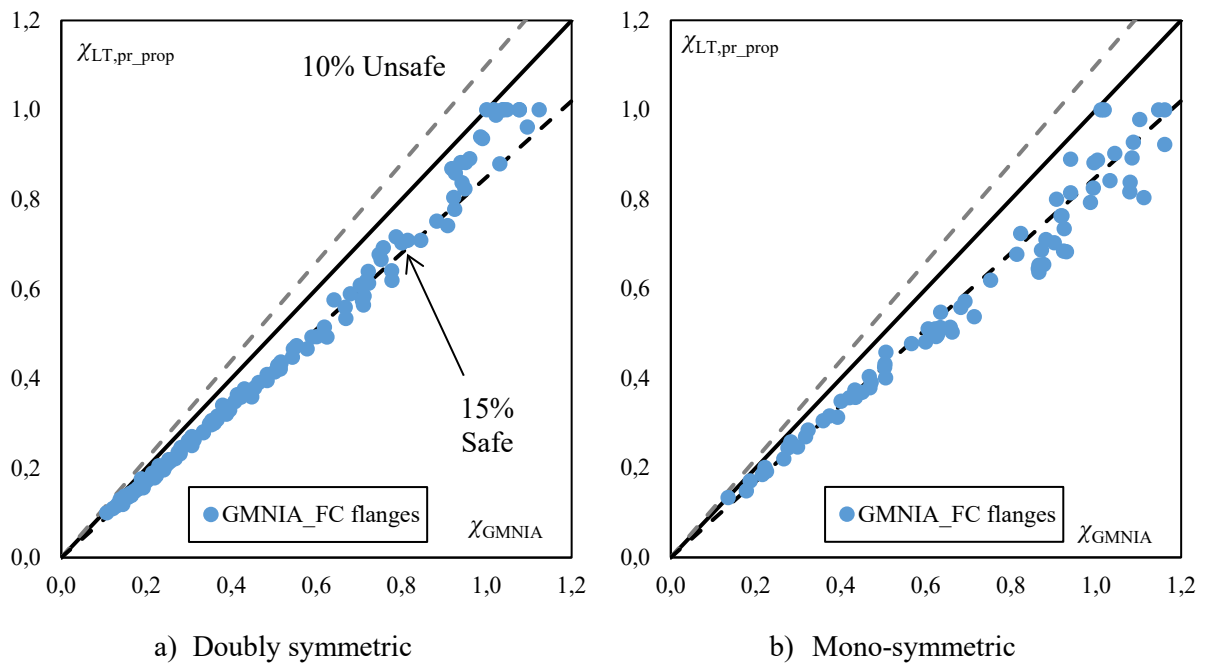
728 **Figure 23: Numerical and *Proposition III* reduction factors for uniform beams under**
 729 **linear bending moment distribution**



730

731 **Figure 24: Numerical and *Proposition III* reduction factors for uniform beams under**
 732 **transverse loading**

733 The partial factors for *Proposition III* are presented in Table 18 and Table 19 for uniform beams
 734 under end moments and transverse loading, respectively. All the partial factors are close to unity,
 735 with values ranging between 0.96 and 1.05.



736

Figure 25: Numerical and *Proposition III* reduction factors for tapered beams

737 Values slightly greater than 1.050 are obtained for low slenderness in the case of uniform mono-
 738 symmetric beams and for medium slenderness in the case of uniform doubly symmetric beams.
 739 Tail approximations are performed, yielding partial factors of 1.02 and 1.01 for doubly symmetric
 740 beams in the intermediate slenderness range and mono-symmetric beams in the low slenderness
 741 range, respectively.

Slenderness range	Doubly symmetric		Mono-symmetric	
	n	γ_{M1}	n	γ_{M1}
$\bar{\lambda}_{LT} \leq 0.8$	107	0.965	62	<u>1.052</u>
$0.8 < \bar{\lambda}_{LT} \leq 1.5$	180	<u>1.052</u>	77	0.977
$1.5 < \bar{\lambda}_{LT}$	100	1.036	57	1.030
All ranges	387	1.078	196	1.042

742 **Table 18: Partial factors of Proposition III for uniform beams subjected to end moments**

Slenderness range	n	γ_{M1}
$\bar{\lambda}_{LT} \leq 1$	40	1.037
$1 < \bar{\lambda}_{LT} \leq 1.5$	55	1.011
$1.5 < \bar{\lambda}_{LT}$	73	0.963
All ranges	168	1.052

743 **Table 19: Partial factors of Proposition III for uniform beams under transverse loading**

744 The partial factors for Proposition III for tapered beams are presented in Table 20. Again, the
 745 values are close to unity and range between 0.96 and 1.04.

Cross-section type	Slenderness range	n	γ_{M1}	
			Proposition III	Proposition III with $g(x_0) = 1$
Doubly symmetric	$\bar{\lambda}_{LT} \leq 0.8$	26	1.039	1.039
	$0.8 < \bar{\lambda}_{LT} \leq 1.5$	42	0.974	0.965
	$1.5 < \bar{\lambda}_{LT}$	61	1.040	1.036
	All ranges	129	1.059	1.053
Mono-symmetric	$\bar{\lambda}_{LT} \leq 0.8$	38	0.956	0.955
	$0.8 < \bar{\lambda}_{LT} \leq 1.25$	28	0.959	0.950
	$1.25 < \bar{\lambda}_{LT}$	29	1.013	1.009
	All ranges	95	0.971	0.968

746 **Table 20: Partial factors for tapered beams**

747 Table 20 also shows the γ_{M1} values obtained with the simplifying assumption that $g(x_0)$,
748 approximated by Eq. (55), is equal to its maximal value, i.e. 1. This safe-sided simplification was
749 motivated by the small changes in the $g(x_0)$ values that range between 0.88 and 1 (see Figure 22a).
750 In addition, this simplification is not associated with a transition zone between uniform and
751 tapered beams. The partial factors obtained assuming $g(x_0) = 1$ are slightly smaller than or equal
752 to those obtained for *Proposition III*, i.e. making use of Eq. (55). The maximal deviation is less
753 than 0.01.
754 The partial factors are all satisfactory in regard to *Proposition III* for tapered and uniform beams
755 with either a doubly or a mono-symmetric cross-section.

756 **4.3 Summary of the proposals**

757 Design methods dedicated to welded beams made of hot-rolled or flame-cut flanges are proposed
758 based on the results of an extensive parametric study which included S275 and S355 uniform and
759 tapered beams with a doubly or mono-symmetric cross-section. Beams were studied under a linear
760 bending moment distribution or subjected to a transverse loading. The latter was applied
761 pointwise at mid-span or uniformly distributed, at the cross-section shear centre or at the centroid
762 of the compression or tension flange. Besides, the dimensions of the members are in line with
763 common practice for steel buildings.

764 The three proposed methods to compute the reduction factor for lateral-torsional buckling χ_{LT} of
765 uniform or web-tapered welded beams with flame-cut flanges with doubly or mono-symmetric
766 cross-sections are summarized in Table 21. *Propositions I* and *II* are based on Eurocode 3 Part 1-
767 1 ([1], [2]) buckling curve approach, with different values for the imperfection factor. Besides,
768 *Proposition II* makes use of factor f accounting for the bending moment distribution while
769 *Proposition I* yields reduction factors which do not depend on the bending moment distribution.
770 *Proposition III* is based on the prEurocode 3 Part 1-1 [1] *new verification method*.

771 Table 21 also presents the method or for computing χ_{LT} for uniform doubly symmetric welded
772 beams with hot-rolled flanges. The partial factors associated with all the proposals are
773 characterized by satisfactory safety levels.

Welded beams with flame-cut flanges

Welded beams with hot-rolled flanges

Proposition I

Proposition II

Proposition III

α_{LT}	0.49	$0.21 \leq \frac{0.23 + 0.10\gamma}{\bar{\lambda}_{LT}} \sqrt{\frac{h_t}{b}} \leq 0.49$	$0.21 \sqrt{\frac{W_{el,y}}{W_{el,z}}} \leq 0.49 + 0.15\gamma$	$0.21 \leq \frac{0.30}{\bar{\lambda}_{LT}} \sqrt{\frac{h_t}{b}} \leq 0.76$
ϕ_{LT}	$0.5 \left[1 + \alpha_{LT} (\bar{\lambda}_{LT} - 0.2) + \bar{\lambda}_{LT}^2 \right]$	$0.5 \left[1 + f_M \left(\left(\frac{\bar{\lambda}_{LT}}{\bar{\lambda}_z} \right)^2 \alpha_{LT} (\bar{\lambda}_z - 0.2) \xi + \bar{\lambda}_{LT}^2 \right) \right]$	$0.5 \left[1 + \alpha_{LT} (\bar{\lambda}_{LT} - 0.2) + \bar{\lambda}_{LT}^2 \right]$	
χ_{LT}	$\frac{1}{\phi_{LT} + \sqrt{\phi_{LT}^2 - \bar{\lambda}_{LT}^2}} \leq 1.0$	$\frac{1/f}{\phi_{LT} + \sqrt{\phi_{LT}^2 - \bar{\lambda}_{LT}^2}} \leq 1.0$	$\frac{f_M}{\phi_{LT} + \sqrt{\phi_{LT}^2 - f_M \bar{\lambda}_{LT}^2}} \leq 1.0$	$\frac{1/f}{\phi_{LT} + \sqrt{\phi_{LT}^2 - \bar{\lambda}_{LT}^2}} \leq 1.0$

Table 21: Proposals for lateral-torsional buckling of welded beams

4.4 Comparison with experimental tests

775
776
777
778
779
780
781

The three *Propositions* for welded beams made of flame-cut flanges developed in the present paper are finally compared against test results. The experimental data from Lebastard et al. [4], Tankova [21], Schaper et al. [22] and Ji et al. [23] for welded beams made of flame-cut flanges are considered. The analytical results are normalized to the experimental results in Table 22 for *Propositions I, II* and *III*. The values obtained using the *General case* from the current and future EN 1993-1-1 ([2], [1]) are also presented for comparison.

Reference	Specimen	F_{EC3}/F_{Exp}	F_{PropI}/F_{Exp}	F_{PropII}/F_{Exp}	$F_{PropIII}/F_{Exp}$
Lebastard et al. [4]	U-DS	0.603	0.691	0.789	0.935
	U-MS	0.553	0.627	0.715	0.852
	T-DS	0.595	0.686	0.780	0.852
	T-MS	0.618	0.707	0.807	0.898
Tankova [21]	B1	0.642	0.732	0.836	0.969
	B2	0.578	0.660	0.753	0.786
Schaper et al. [22]	Pos. 1	0.705	0.705	0.839	0.751
	Pos. 1f _y	0.636	0.636	0.733	0.664
	Pos. 3-1	0.722	0.811	0.938	0.812
	Pos. 3-1f _y	0.594	0.664	0.762	0.671
	Pos. 3-2	0.738	0.738	0.855	0.770
	Pos. 4-1	0.773	0.773	0.872	0.779
	Pos. 5	0.654	0.756	0.893	1.018
Ji et al. [23]	Pos. 14	0.639	0.725	0.847	0.816
	G6-430-32-1-f	0.629	0.629	0.750	0.669

782

Table 22: Analytical and Experimental ultimate loads

783
784
785
786
787
788

Ratios between the current rules and experimental values are between 0.55 and 0.77 with few results greater than 0.65. *Proposition I* produces increased values for the analytical results except for stocky members. The ratios range between 0.63 and 0.81. Making use of *Proposition II* provides greater analytical resistance, with ratios between 0.72 and 0.94. These values are close to those obtained using *Proposition III*, which range between 0.66 and 0.97, except for Pos. 5 from Schaper et al. [22], for which a ratio of 1.02 is found.

789 It is worth recalling that the experimental set up of Schaper et al. [22] included a load jack applied
790 upwards at mid-span. However, to control the buckling direction, the load was applied with a
791 small eccentricity with respect to the web, thus enforcing an additional torsional moment. This
792 effect is not accounted for in the analytical computations of Table 22 and explains the non-
793 conservative result obtained for the mono-symmetric beam Pos. 5 with *Proposition III*. The
794 greatest value of B_{Ed}/B_{Rk} is obtained for this beam and is equal to 0.15, reducing the bending
795 moment capacity. The values of B_{Ed}/B_{Rk} are lower for the remaining tests performed by Schaper
796 et al. [22], i.e. up to 0.07.

797 While the maximal deviation from the experimental result is nearly 50% when using the Eurocode
798 3 design method, it is reduced to 28% and 34% when using *Propositions II* and *III*, respectively.
799 Besides, only two and three results obtained with *Propositions II* and *III*, respectively, show a
800 deviation from experimental results of greater than 25%. The largest deviations are observed for
801 specimens Pos. 1f_y, Pos. 3-1f_y and G6-430-32-1-f. The numerical ultimate loads showed the
802 largest deviations on the safe side – 6% to 9% – from the experimental failure loads for these
803 beams [4]. The actual geometrical imperfections and residual stresses were slightly more
804 favourable than those introduced in the numerical model.

805 *Proposition I* does not account for the bending moment distribution and is associated with a single
806 buckling curve for all beams. This design method is consequently less accurate than the two others
807 and yields more conservative results with a maximal deviation of 37%.

808

809 **5 CONCLUSIONS**

810 Using a numerical model validated against experimental tests, a parametric study was conducted
811 focusing on the lateral-torsional buckling behaviour of welded beams. The parametric study
812 included S275 and S355 uniform and tapered beams, with a doubly or mono-symmetric cross-
813 section. The maximum cross-section depth varied between 250 and 1000 mm while the flanges
814 widths ranged between 100 and 350 mm. For mono-symmetric beams, the ratios between the
815 thickness of both flanges and/or their widths was up to 2. The beams were analysed under a linear
816 bending moment or under a transverse loading. The latter was uniformly distributed over the
817 length or applied pointwise at mid-span, at the level of the cross-section shear centre or the
818 centroid of the compressive or tensile flange. Most of the studied specimens were made of flame-
819 cut flanges and completed with specimens made of hot-rolled flanges. Uniform and tapered
820 members with a doubly or mono-symmetric cross-section were studied. The comparison between
821 the numerical and analytical results highlighted that the use of buckling curve d , commonly
822 prescribed in the *General case* from Eurocode 3 and prEurocode 3 Part 1-1 ([1], [2]), is
823 excessively conservative for welded beams made of flame-cut flanges. The corresponding partial
824 factors being significantly lower than unity confirm these observations. This design method is
825 also very conservative for welded beams with hot-rolled flanges having a medium-to-high
826 slenderness. The *new verification format* of prEN 1993-1-1 [1] provides more accurate predictions
827 of the buckling resistance for beams with hot-rolled or flame-cut flanges with a safety margin,
828 but only applies to uniform doubly symmetric beams.

829 Therefore, adaptations of the *General case* were proposed for welded beams made of flame-cut
830 flanges for steel buildings. First, a simple proposal consists in using buckling curve c . A second
831 proposal introduces an imperfection factor inversely proportional to the slenderness and
832 depending on the cross-section depth-to-width ratio as well as on the tapering of the member. This
833 imperfection factor comes with upper and lower bounds corresponding to buckling curves a and
834 c , respectively. This second proposal also includes a factor explicitly accounting for the bending
835 moment distribution when computing the lateral-torsional buckling resistance owing to a visible

836 influence on the numerical results. The second proposal yields more accurate lateral-torsional
837 buckling resistances than the first proposal. Partial factors were computed for both proposals and
838 were satisfactory for all of the beam types studied. The second proposal is also adapted to the case
839 of uniform doubly symmetric welded beams with hot-rolled flanges. The expression for the
840 imperfection factor is slightly modified with a lower bound corresponding to buckling curve *d*.
841 Since the scope of the *new verification format* is restricted to uniform doubly symmetric beams,
842 an extension of this design method to tapered mono-symmetric beams was investigated. The
843 mechanical bases and assumptions employed to develop this design method ([8], [9]) were
844 considered in the analytical derivations of the present paper. The resulting method is similar to
845 that from prEurocode 3 [1] with a few adjustments. A new term is introduced accounting for the
846 tapering and mono-symmetric design of the beam. An imperfection factor adapted to welded
847 beams with $t_f \leq 40$ mm and made of flame-cut flanges is also proposed. The corresponding partial
848 factors are again adequate for tapered and uniform beams with a doubly or mono-symmetric cross-
849 section. A clear safety margin from experimental results extracted from the literature ([4], [21],
850 [22] and [23]) is obtained for the three proposals for welded I-section beams made of flame-cut
851 flanges.

852 Uniform and tapered beams with a doubly or mono-symmetric cross-section were investigated
853 with flame-cut flanges while the studied welded beams with hot-rolled flanges were only uniform
854 and doubly symmetric. The parametric study of welded beams made of hot-rolled flanges should
855 be extended to cover a wider scope. Distinct design methods could then be obtained for uniform
856 or tapered welded beams made of hot-rolled or flame-cut flanges with a doubly or mono-
857 symmetric cross-section. Plasma-cut flanges commonly used in practice should also be
858 investigated.

859

860 **6 REFERENCES**

- [1] CEN/TC 250. (2021) *prEN 1993-1-1: Eurocode 3 – Design of steel structures – Part 1-1: General rules and rules for buildings*. CEN/TC 250/SC 3/WG 1 – Draft version.
- [2] CEN. (2005) *EN 1993-1-1: Eurocode 3 – Design of steel structures – Part 1-1: General rules and rules for buildings*. European Committee for Standardization.
- [3] ECCS, Committee 8 – Stability. (1976) *Publication n°22: Manual on stability of steel structures*.
- [4] Lebastard, M.; Couchaux, M. Bureau, A.; Hjiiaj, M. (2023) *Impact of the fabrication process on the lateral-torsional buckling of welded I-section beams*. *Thin-Walled Structures*, vol. 188, 110761.
- [5] CEN/TC 250. (2021) *prEN 1993-1-14: Eurocode 3 – Design of steel structures – Part 1-14: Design assisted by finite element analysis*. CEN/TC 250/SC 3 – prEN 1993-1-14 – Draft version.
- [6] CEN. (2003) *EN 1990: Eurocode 0 – basis of structural design*. European Committee for Standardization.
- [7] SAFEBRITILE: Standardization of Safety Assessment Procedures across Brittle to Ductile Failure Modes (2017). *Final Report*. Grant Agreement Number RFSR-CT-2013-00023.
- [8] Taras, A. (2010) *Contribution to the development of consistent stability design rules for steel members*. PhD thesis, Technical University of Graz, Austria.
- [9] Taras, A.; Greiner, R. (2010) *New design curves for lateral-torsional buckling – Proposal based on a consistent derivation*. *Journal of Constructional Steel Research*, vol. 66, pp 648-663.
- [10] Marques, L.; Simões da Silva, L.; Rebelo, C.; Santiago, A. (2014) *Extension of EC3-1-1 interaction formulae for the stability verification of tapered beam-columns*. *Journal of Constructional Steel Research*, vol. 100, pp 122-135.

- [11] Tankova, T.; Simões da Silva, L.; Marques, L. (2018) *Buckling resistance of non-uniform steel members based on stress utilization: General formulation*. Journal of Constructional Steel Research, vol. 149, pp 239-256.
- [12] Sfintesco, D. (1970) *Fondement expérimental des courbes européennes de flambement*. Revue Construction Métallique, n°3, pp 5-12.
- [13] Maquoi, R.; Rondal, J. (1978) *Mise en équation des nouvelles courbes européennes de flambement*. Revue Construction Métallique, n°1, pp 17-30.
- [14] Rondal, J.; Maquoi, R. (1979) *Formulations d'Ayrton-Perry pour le flambement des barres métalliques*. Revue Construction Métallique, n°4, pp 41-53.
- [15] AFNOR. (2013) *NF EN 1993-1-1/NA: Eurocode 3 – Design of steel structures – Part 1-1: General rules and rules for buildings – French national Annex to EN 1993-1-1*.
- [16] ECCS, Technical Committee 8 – Structural stability (1984) *Publication n°33: Ultimate limit state calculation of sway frames with rigid joints*.
- [17] CEN. (2007) *EN 1993-1-5: Eurocode 3 – Design of steel structures – Part 1-5: Plated structural elements*. European Committee for Standardization.
- [18] Couto, C.; Vila Real, P. (2019) *Numerical investigation on the influence of imperfections in the lateral-torsional buckling of beams with slender I-shaped welded sections*. Thin-Walled Structures, vol. 145, 106429
- [19] Gérard, L.; Li, L.; Kettler, M.; Boissonnade, N. (2019) *Recommendations on the geometrical imperfections definition for the resistance of I-sections*. Journal of Constructional Steel Research, vol. 162, 105716.
- [20] Boissonnade, N.; Somja, H. (2012) *Influence of Imperfections in FEM Modeling of Lateral Torsional Buckling*. Proceedings of the Annual Stability Conference – Structural Stability Research Council, Grapevine, USA.
- [21] Tankova, T. (2018) *Stability design of columns, beams and beam-columns: behaviour, general formulation and reliability*. PhD thesis, Universidade de Coimbra, Portugal.

- [22] Schaper, L. Jörg, F.; Winkler, R.; Kuhlmann, U.; Knobloch, M. (2019) *The simplified method of the equivalent compression flange*. Steel Construction, vol. 12, n°4, pp 264-277.
- [23] Ji, X.L.D.; Twizell, S.; Driver, R.; Imanpour, A. (2022) *Lateral Torsional Buckling Response of Compact I-shaped Welded Girders*. Journal of Structural Engineering, vol. 148, n10, 04022149.
- [24] CEN/TC 250 (2020) *prEN 1990: Eurocode – Basis of structural design and geotechnical design*. CEN/TC 250 – prEN 1990 – Draft version.
- [25] Kitipornchai, S.; Trahair, N. (1972) *Elastic stability of tapered I-beams*. Journal of the Structural Division, vol. 98, n°3, pp 713-728.
- [26] Kitipornchai, S.; Trahair, N. (1975) *Elastic behaviour of tapered monosymmetric I-beams*. Journal of the Structural Division, vol. 101, n°8, pp 1661-1678.
- [27] Thiébaud, R. (2014) *Résistance au déversement des poutres métalliques de pont*. PhD thesis, Ecole polytechnique fédérale de Lausanne, Switzerland.
- [28] Tankova, T.; Simões da Silva, L.; Rodrigues, F. (2022) *Buckling curve selection for HSS welded I-section members*. Thin-Walled Structures, vol. 177, 109430.